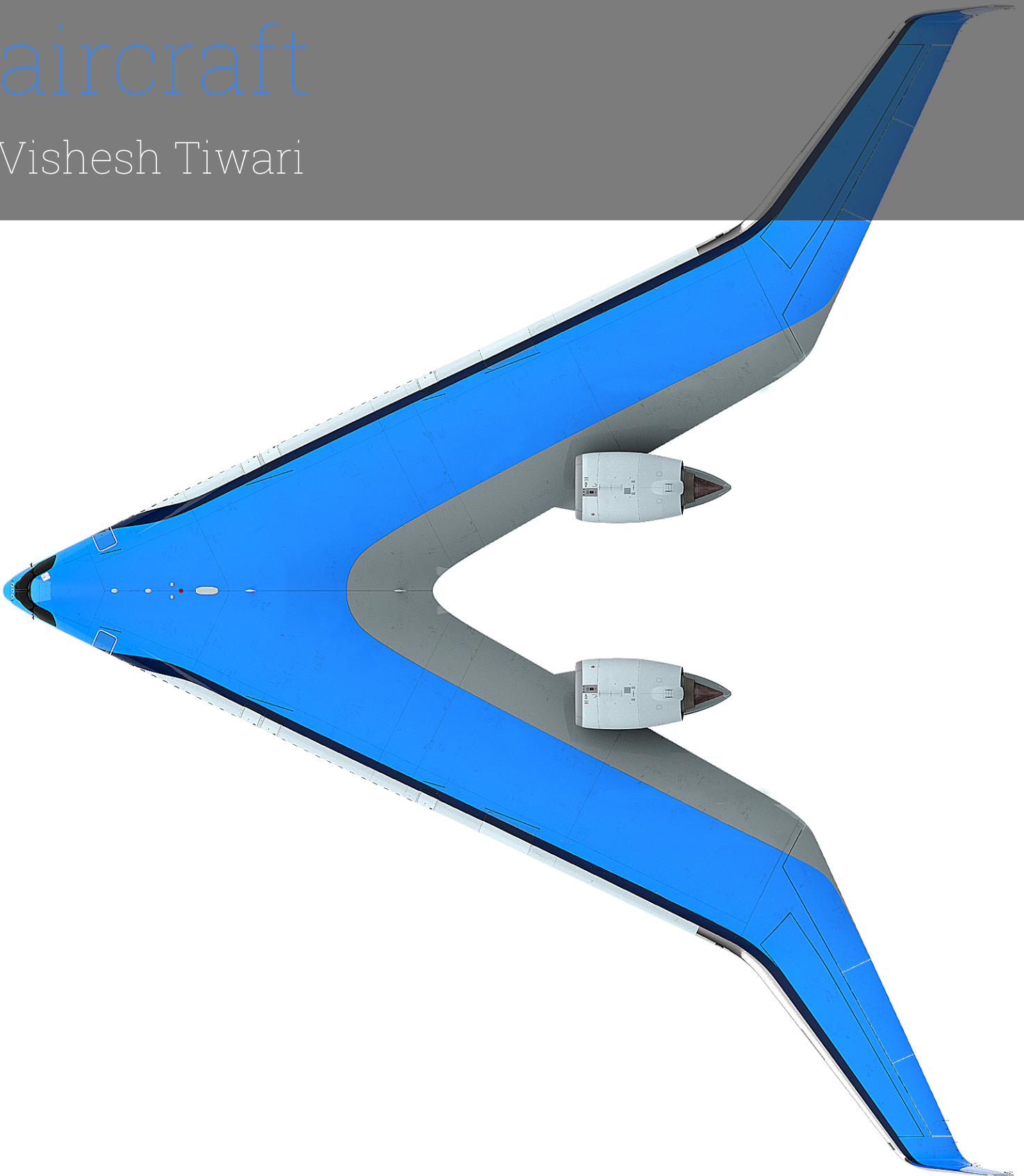


Sizing of control surfaces on a Flying V aircraft

Vishesh Tiwari



Sizing of control surfaces on a Flying V aircraft

by

Vishesh Tiwari

Student Name	Student Number
Vishesh Tiwari	5805953

Project Duration: January 8, 2024 - May 28, 2025

Thesis committee: Dr. ir. R. Vos

Dr. C. Varriale

Dr. ir. E. van Kampen

Guide: Dr. S. Asaro

Faculty: Faculty of Aerospace Engineering, Delft

TU Delft, Supervisor

TU Delft, Chair

TU Delft, Examiner

Preface

This document is meant to be the final deliverable of the Master thesis, the final step in completing the graduation process. This work is culmination of research and work done in previous year, using the knowledge gained in the extensive coursework done in the first year. Completing this thesis would not have been possible without the consistent support of my friends and family, especially my mother and sister, to whom I am always grateful.

Finally, I would like to thank Prof. Vos and Dr. Salvatore Asaro for providing me the opportunity to work on such an interesting topic, and supporting me at times when I struggled from personal or academic difficulties.

Vishesh Tiwari
Delft, May 2025

Abstract

The goals of governments and agencies around the world is to minimize fuel emissions for the upcoming decades. The Flying V offers a new concept, which is an aircraft of flying wing configuration, offering higher aerodynamic efficiency than conventional tube and wing configuration. However, such an configuration offers challenges with its stability and control characteristics, with difficulties arising in control authority, like for instance, longitudinal trim. This study aims to find the optimal control surface layout for the FV-1000 aircraft. First, the certification requirements relevant to each control surface to be sized in this study (aileron, elevator and rudder) are gathered, primarily based on CS-25 regulations, and they are expressed mathematically. AVL is chosen as the tool to conduct aerodynamic analysis, for sizing purposes. Two coefficients are compared for their viability as objective function for optimizing a control surface, C_{HM} and C_D , C_{HM} turns out to be the better option, it also provides control surface for a given span as small as possible. A consistent optimization framework is applied to both the aileron and elevator, wherein the spanwise domain is discretized and various combinations of span length and hinge line chord percentage are evaluated. The resulting optimal configurations are spatially adjacent, with the sizing of each control surface constrained by the span available due to presence of the other. During validation procedure, the comparisons made between VLM and wind-tunnel when extrapolated to comparison between VLM analysis and full scale flight case, it is observed that aileron is oversized, (for time to bank) while control elevators are undersized (to be precise, for pull-up maneuver). Certain solutions like high-lift devices or other methods of reducing AoA are suggested to make control surface like elevator comply with requirements. Rudders are the final surface to be sized which satisfy requirements of OEI trim at VLM analysis and even for full scale case, but is not able to satisfy the Steady sideslip requirement by significant margin for both cases. However, these results signify need of research on other options to assist these control surfaces, like drag rudders to assist with directional control authority, high lift devices to decrease AoA, assist surfaces like elevator in meeting the certification requirement, which are discussed.

Contents

Preface	i
Nomenclature	viii
1 Introduction	1
1.1 Problem statement:	2
1.2 Thesis Outline:	2
2 Background	3
2.1 Flying V	3
2.2 Theoretical background for aerodynamic analysis	9
2.2.1 Biot-Savart Law	9
2.2.2 Prandtl Classical Lifting line theory	10
2.2.3 Vortex Lattice method- VLM	12
2.2.4 Trefftz Plane-far field analysis	13
3 Methodology	15
3.1 Athena Vortex Lattice- AVL	15
3.2 Certification requirements for control authority	16
3.2.1 Longitudinal Trim	17
3.2.2 Lateral control:Time-to-bank	17
3.2.3 Steady Sideslip	18
3.2.4 One- Engine Inoperative (OEI) trim	19
3.2.5 Longitudinal- Pull-up Maneuver	19
3.2.6 Take-off rotation speed:	20
3.2.7 High Angle of attack departure: Lateral Control Departure Parameter (LCDP) & $C_{n_{\beta_{DYN}}}$	20
3.3 Initial optimization- objective function-selection	21
3.4 Method adopted for control surfaces	25
4 Validation	29
4.1 Stability and Control derivatives	29
4.2 Center of Gravity range determination	32
5 Results	35
5.1 Aileron-sizing	35
5.1.1 Selection of α_{trim}	35
5.1.2 Sizing at the selected α_{trim}	36
5.2 Elevator sizing	39
5.3 Rudder sizing	43

6 Conclusion and Recommendations 48
6.1 Conclusion 48
6.2 Recommendations: 49

References 51

List of Figures

1.1	Initial artistic impression of Flying V [7]	1
2.1	Changes made from initial conceptual to preliminary design	4
2.2	Elevon design opted by Cappuyns[10] for handling quality analysis	5
2.3	Stability Augmentation system opted by Joosten[26]	6
2.4	Control surface design opted by Tooren[42]	7
2.5	Rudder parameterization used by Amur[3] for winglet optimization	8
2.6	Vortex filament induction at a point	9
2.7	Visualization of vortex and induced drag concepts [4]	10
2.8	Infinite Horseshoe vortices on lifting line [4]	10
2.9	Horse-shoe vortex system on a finite wing [4]	12
2.10	Flow tangency condition at a control point- influenced by rotation of vector by deflection[15]	13
2.11	Trefftz plane analysis for induced drag, with focus on perturbations caused in the Trefftz plane [15]	13
3.1	Geometry of Flying-V analyzed in AVL	16
3.2	Elevator's area of domain used for initial optimization trial	23
3.3	Optimized elevators-results of initial optimization:a) Constant chord fraction ;b) Different chord fraction	24
3.4	Representative domain for sizing the control surface;divisions or cells highlighted via dashes	26
3.5	Flowchart- optimization algorithm for control surface(aileron,elevator)	27
4.1	Half-Flying-V section used for wind tunnel experiment [34]	29
4.2	Flying V subscale model for flight test experiment [19]	29
4.3	Steady-sideslip trim at a sideslip angle; Sideslip angle(β) vs. Control deflection(δ_r & δ_a) deflection comparison- Experimental & VLM-based data	32
4.4	C_m vs α for various C.G. positions	33
4.5	Loading diagram or C.G. Envelope	34
5.1	Domain for sizing the aileron;divisions or cells highlighted via dashes	36
5.2	Optimized aileron, designed at $\alpha_{trim} = 17.98^\circ$	38
5.3	Domain for sizing the elevator;divisions or cells highlighted via dashes	40
5.4	Elevator and aileron design- optimized combination	41
5.5	Elevator and aileron design- optimized combination, aileron's hingeline matched to ele- vator's hingeline	42
5.6	Two-dimensional side-view of Rudder designs with hinge line at chord fraction-0.6(red) & 0.7(blue)	44

5.7 Comparison of deflections (absolute values) for OEI trim condition at forward CG ($x_{cg} = 30.15$ m) & aft CG ($x_{cg} = 31.15$ m) 45

5.8 Deflections(absolute values) for steady sideslip condition at aft CG ($x_{cg} = 31.15$ m) & aft CG ($x_{cg} = 31.15$ m) 45

List of Tables

3.1	Certification requirements - tabulated	21
3.2	Results of initial optimization cases	24
4.1	Comparison of Wind-tunnel and VLM results for different angles of attack of $C_{m_{\delta_e}}$	30
4.2	Comparison of $C_{m_{\alpha}}$ values: Experimental vs. VLM at $\alpha = 7.5^\circ$	30
4.3	Comparison of Coefficient Derivatives: Experimental vs VLM	31
4.4	Deflection of rudder and aileron in subscale for $\beta = 9.83^\circ$, for steady sideslip	32
4.5	FV-1000- component weight information [33]	33
5.1	Effect of Aileron Span on Bank Angle Over 7 Seconds	36
5.2	Effect of Elevator Span on Trimmed Angle of Attack and Elevator Deflection	39
5.3	Deflection angle at various AoAs for chord fraction=0.7, at forward CG ($x_{cg} = 30.15$), V_{mc} , mass-MTOW	46

Nomenclature

Abbreviations

Abbreviation	Definition
ISA	International Standard Atmosphere
CG	Center of Gravity
MLW	Maximum Landing Weight
MTOW	Maximum Take-Off Weight
VLM	Vortex Lattice Method
AoA	Angle of Attack
OEI	One Engine Inoperative

Symbols

Symbol	Definition	Unit
V	Velocity	[m/s]
V_{app}	Approach velocity	[m/s]
b	Wingspan	[m]
q	Dynamic pressure	[N/m ²]
I_{XX}	Moment of inertia about x-axis	[Kg m ²]
y_{eng}	Spanwise position of engine	[m]
$C_{n_{OEI}}$	Yawing moment coefficient due to asymmetric thrust in OEI condition	[m]
c	Chord length	[m]
x/c	Chord fraction	[]
\bar{c}	Mean aerodynamic chord	[m]
C_L	Lift coefficient	[-]
C_{L_0}	Lift coefficient at zero AoA and control deflection	[-]
C_{L_α}	Lift curve slope	[1/rad]
$C_{L_{\delta_e}}$	Change in lift coeff. due to elevator deflection	[1/rad]
C_{L_q}	Pitch rate derivative of lift coefficient	[-]
C_m	Pitching moment coefficient	[-]
C_{m_0}	Zero AoA and zero deflection pitching moment coefficient	[-]
C_{m_α}	Pitching moment derivative w.r.t. AoA	[1/rad]
$C_{m_{\delta_e}}$	Change in moment coeff. due to elevator deflection	[1/rad]
C_{m_q}	Pitch rate derivative of pitching moment coefficient	[-]

Symbol	Definition	Unit
C_l	Rolling moment coefficient	[-]
$C_{l\beta}$	Rolling moment derivative w.r.t. sideslip	[-]
$C_{l\delta_a}$	Aileron effectiveness in roll	[-]
$C_{l\delta_r}$	Rudder effect on roll moment	[-]
C_{l_p}	Roll damping derivative	[-]
C_Y	Side force coefficient	[-]
$C_{Y\beta}$	Side force derivative w.r.t. sideslip	[-]
$C_{Y\delta_r}$	Rudder side force effectiveness	[-]
$C_{Y\delta_a}$	Aileron side force effectiveness	[-]
C_n	Yawing moment coefficient	[-]
$C_{n\beta}$	Yaw moment derivative w.r.t. sideslip	[-]
$C_{n\delta_a}$	Aileron effect on yaw moment	[-]
$C_{n\delta_r}$	Rudder effectiveness in yaw	[-]
L_p	Roll mode stability derivative	[-]
n	Load factor	[-]
N_{OEI}	Yawing moment due to OEI	[N·m]
S	Reference wing area	[m ²]
T_{TO}	Takeoff thrust of one engine	[N]
t	Time	[s]
V_{MO}	Maximum operating limit speed	[m/s]
V_{SR1}	Stall speed in landing configuration	[m/s]
V_{mc}	Minimum control speed	[m/s]
W	Aircraft weight	[N]
\dot{p}	Roll rate derivative	[rad/s ²]
$\dot{\phi}$	Time derivative of bank angle	[rad/s]
\hat{q}	Non-dimensional pitch rate	[-]
L'	Lift per unit span	[N/m]
ρ	Density	[kg/m ³]
Γ	Circulation strength	[m ² /s]
ϕ	Bank angle	[degrees,°]
$\nabla\phi$	Perturbation velocity	[m/s]
δ_e	Elevator deflection angle	[degrees[°] or radians]
δ_a	Aileron deflection angle	[degrees[°] or radians]
...		

1

Introduction

The aviation industry in recent decades has been growing consistently, but with growth comes an increase in emissions. Governments and agencies around the world have taken cognizance of this and are committing to a sustainable future, for example, "Flightpath 2050"[12] is a vision defined by the European Union for aviation industry, which also focuses on sustainability, for instance, it aims to reduce the CO_2 emission per passenger kilometer. In terms of technical developments, the design of new advanced aircraft must be researched, developed and integrated in the next 30 years[1]. The Flying-V is a commercial transport aircraft, which was proposed by Benad[7] in 2015, which has an unconventional flying wing configuration, as can be seen in figure 1.1. This proposed design was compared with the aircraft A350-900, which has the same capacity, initial estimates predicted 10% higher aerodynamic efficiency, and empty weight lower by 2%. In the winglet and rudder design study done by Horwitz[23], a study into aerodynamic analysis of control surface like the rudder is suggested for further research.

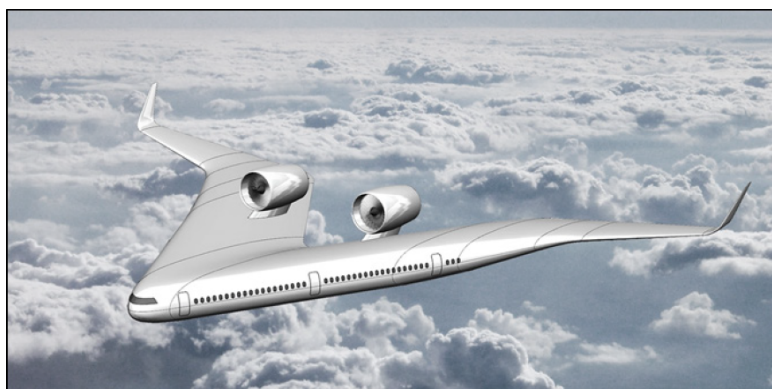


Figure 1.1: Initial artistic impression of Flying V [7]

Although the flying wing configuration promises higher aerodynamic efficiency, it is more prone to stability and maneuvering issues compared to the conventional tube-and-wing design. The preliminary design of the layout of the control surface at the trailing edge of the outer wing was carried out using the A350-900 aircraft as reference by Palermo[34], but was not further optimized. Cappuyns[10] de-

signed a control surface that covers the entire trailing edge of outer wing ,with a split introduced in an arbitrary position, identifying deficiencies in the lateral-directional capability of Flying-V.

1.1. Problem statement:

The research in this dissertation is thus mainly focused on sizing the control surface and eventually propose a layout for the Flying V. The purpose of this study in terms of research objective can be framed as follows: *"to size and propose a control surface layout for the flying-V aircraft (specifically FV-1000) with help of aerodynamic analysis to obtain the required aerodynamic coefficients, such that the resulting control surface abides the certification requirements for each type of control surface"*. This objective can be stated in a more broader terms in form of the following main research question to be looked into:

"What is the optimal sizing and layout of control surfaces for the Flying-V aircraft?" This research question, although it captures the essence of what needs to be done to achieve the research objective, this study requires to pose such a broad research question into sub-questions, which need to be answered. The sub-questions are as follows:

- How should the trailing-edge control surfaces on the outer wing be allocated between elevator and aileron functions?(how to split trailing edge control surface)
- What is an appropriate approach to optimizing control surface sizing and allocation, in terms of design variable selection and discretization of the design domain?
- Which control authority requirements are most limiting when designing control surfaces that must satisfy multiple constraints?

While sizing surfaces, all the relevant constraints in terms of geometrical and structural constraints must be considered, for instance spar position or fuel tank position. The control authority requirements can be taken from those prescribed by regulatory bodies like CS-25 by EASA [2].

1.2. Thesis Outline:

The objective of this thesis being stated, a brief explanation of the layout of this thesis is to be provided. First comes the background chapter, in which a brief account of relevant work that has already been done until now on Flying V is given, after which the theoretical background of VLM-Vortex Lattice Method is given which explains the fundamental physics of the applied analysis tool for this study. The next chapter is methodology which provides the methods opted to achieve the optimal sizing of control surfaces. The results of utilizing the methods discussed previously are provided in this section, also with some explanations about how they were obtained. Finally, the conclusions and recommendations include a short summary of all the important results of the study, some shortcomings or gaps to be filled, and recommendations for future work in the control surface related to Flying-V are given.

2

Background

This chapter, in the first section-'Flying V' includes the information about development of Flying-V, with a focus on development of control surfaces or handling quality assessment studies. After that fundamental details of concepts which are applied in VLM, used for aerodynamic analysis in this study are discussed in the second section.

2.1. Flying V

The Flying-V design was originally proposed by J. Benad in 2015[7], and has been an ongoing project at TU Delft since 2016. The flying wing configuration does promise higher aerodynamic efficiency, due to the larger laminar flow area compared to predominantly turbulent conventional tube and wing configuration[41], but at the same time, this configuration is prone to having difficulties in stability, maneuvering, control, for example, difficulty in longitudinal trim[30].

The initial design proposed by Benad has gone through several design changes over the years. Faggiano[18] conducted an aerodynamic optimization study, which took the conceptual design of Flying-V by Benad to the preliminary stage. In terms of cabin cross section, changes were made in the cabin cross section from initial cylindrical cross section to oval cross section to provide flexibility, and ensure fulfillment of the cabin requirements. The change in the wing planform from Faggiano's optimization can be observed in figure 2.1, the outboard sweep angle is increased to counter formation of shockwave and profile was modified to increase efficiency.

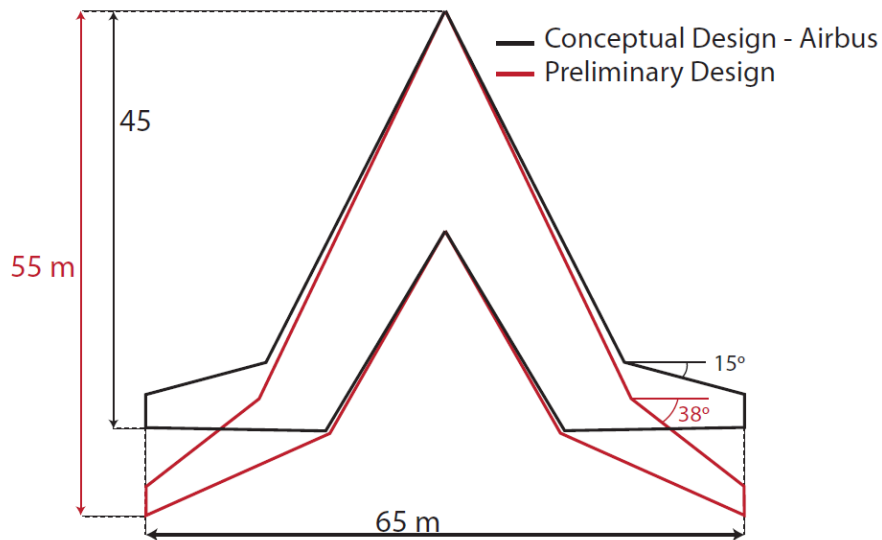


Figure 2.1: Changes made from initial conceptual to preliminary design

The fins were designed to minimize drag, while fulfilling three conditions- directional stability, OEI condition and maximum crosswind landing. The fixed chord of rudder was kept as 0.3 and extending entire fin span. To take the resulting rudder under consideration, it was the OEI condition which was found more limiting than the maximum crosswind condition.

Palermo[35] in his study of longitudinal stability and control characteristics of subscale Flying-V model, determined size of control surface by using A350-900 as reference, and the control surface spans over the entire trailing edge of aircraft after the first kink (over the second and third trunk). A 16% increase control surface volume of Flying-V control surface is noticed in comparison to A350-900, for the proposed control surface configuration. However, decrease in control authority, worst was observed for forward CG positions, where maximum lift coefficient decreased by 20%, with reduction in usable control authority.

Cappuyns[10] in his thesis, researched into handling quality of the Flying V. The certification requirements used in the study comprised of requirements or regulation from EASA CS-25 and MIL-HDBK-1797A (by U.S, military). A 6-DOF flight mechanics toolbox was used to simulate the flight dynamics characteristics of the aircraft and also to simulate trim conditions and obtain the required eigenvalues. The control surfaces used by Cappuyns, are chosen with aim of keeping design simple, not too many surfaces incorporated in trailing edge, only two elevons taken with split position being selected randomly. This control surface layout can be seen in Figure 2.2. In this study Yaw- Stability Augmentation System, pitch controller and control mixer(trailing edge surfaces acting as elevator and aileron both) all are integrated into the control surface.

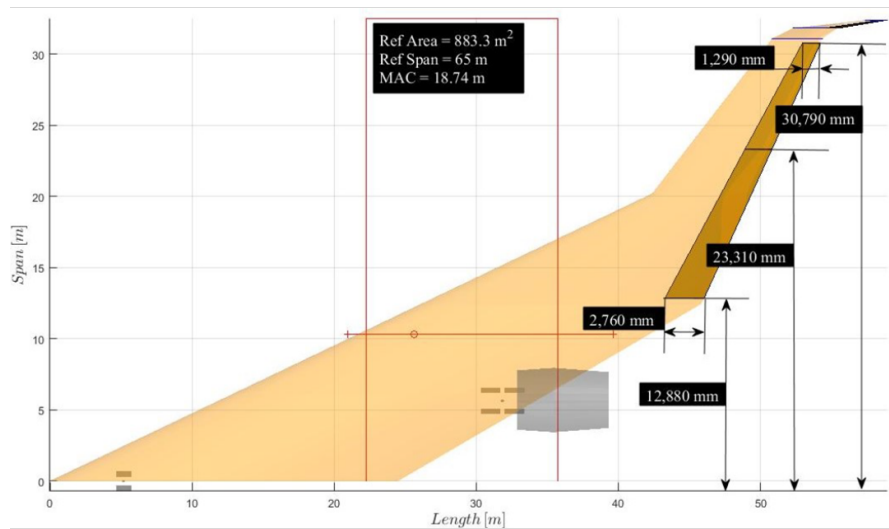


Figure 2.2: Elevon design opted by Cappuyns[10] for handling quality analysis

Considering the results for longitudinal control authority, for the trim at approach condition (MLW, forward CG), the AoA comes out to be within the limits (18°) and elevon deflections as well. When considering both elevons, δ_e comes to be 7.8° and increases to 13° for just one elevon. The other maneuver for assessing longitudinal control authority is pull-up. This maneuver sets limits on the forward CG position (moved from 35% to 45% MAC), so that Flying-V can execute 1.3 g pull up, aircraft weighing at MLW, speed being approach speed. The deflection of elevon (both) for pull-up execution came out to be 14° . Thus, the elevon design seem enough for the longitudinal control requirements, but with a limit imposed on forward CG position.

In context of lateral and directional control authority, when bank to bank maneuver was considered, for All- Engine operative condition, even with using one elevon bank to bank time came out to be 6.1 seconds (under the 7 second limit), only one elevon was deflected to 20° within limits. However, while countering the sideslip during this maneuver by yaw SAS, rudder reached deflection angle of 60° , exceeding the maximum rudder angle. Thus, exceeding rudder deflection makes the design non-compliant. Horwitz [23] conducted parametric design study of winglet, where $C_{n_{\delta_r}}$ values of the Flying-V are compared with a reference transport aircraft, whose $C_{n_{\delta_r}} = -0.098$. In case of Flying-V with a winglet length of 12 m, $C_{n_{\delta_r}} = -0.0044$, thus this value falls short by a substantial margin in matching the $C_{n_{\delta_r}}$ value of reference aircraft. This indicated lack in directional control authority, and further research in this area was recommended, with a disclaimer that there is likely to be an error in calculation of this coefficient ($C_{n_{\delta_r}}$). Joosten [26] study on lateral directional handling quality, where the same design of control surface as Cappuyns was used for analysis, as illustrated in Figure 2.2. In conjunction to stability and control analysis of bareframe aircraft, Stability Augmentation system is also designed and utilized, the system is shown in schematic diagram in Figure 2.3. Control allocation system, with yaw damper, roll damper and sideslip angle feedback are part of this system, to improve the handling quality of control surface design by Cappuyns.

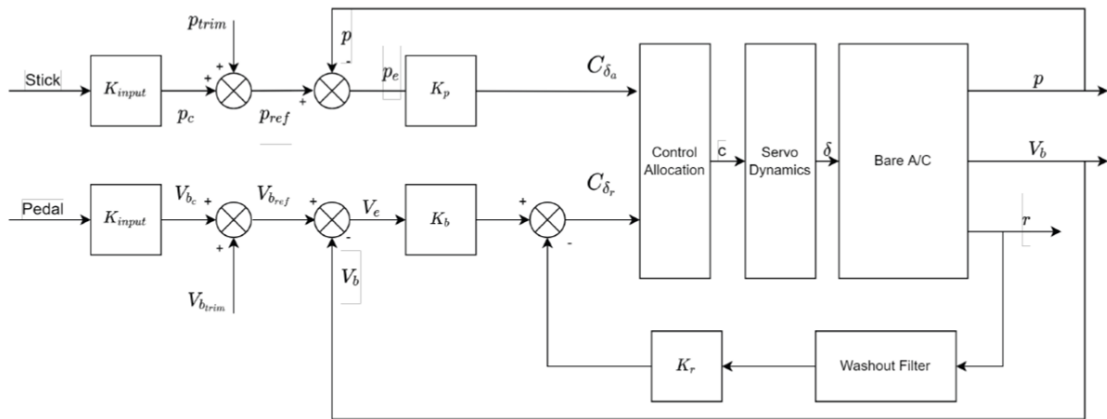


Figure 2.3: Stability Augmentation system opted by Joosten[26]

Dutch roll stability improved with application of SAS, control allocation helped in decreasing the deflection of control surfaces for the certification requirements. However, the implementation of this designed prototype of control system did not fulfill all the certification requirements, like for instance the rudder deflection exceeding by 4 degrees for time to bank requirement for take-off-OEI conditions. Moreover, the SAS is not able to achieve compliance in context of achieving trim in forward CG configuration, approach speed. The roll control authority is also not enough to fulfill maneuverability requirements such as time to bank.

While most of the studies until Tooren's study [42] were focused on optimization in terms of aerodynamic efficiency, stability and control constraints were not considered in detail while forming these designs. This study explored the effect of stability and control requirements on fuel efficiency, and how the aerodynamic stability and control derivatives are effected by design aspects. The control surface design opted in this study is illustrated in Figure 2.4. There is no sizing done for the control surface chord fraction at ends only their value is given, as it was design variables of aircraft which were of interest in the optimization.

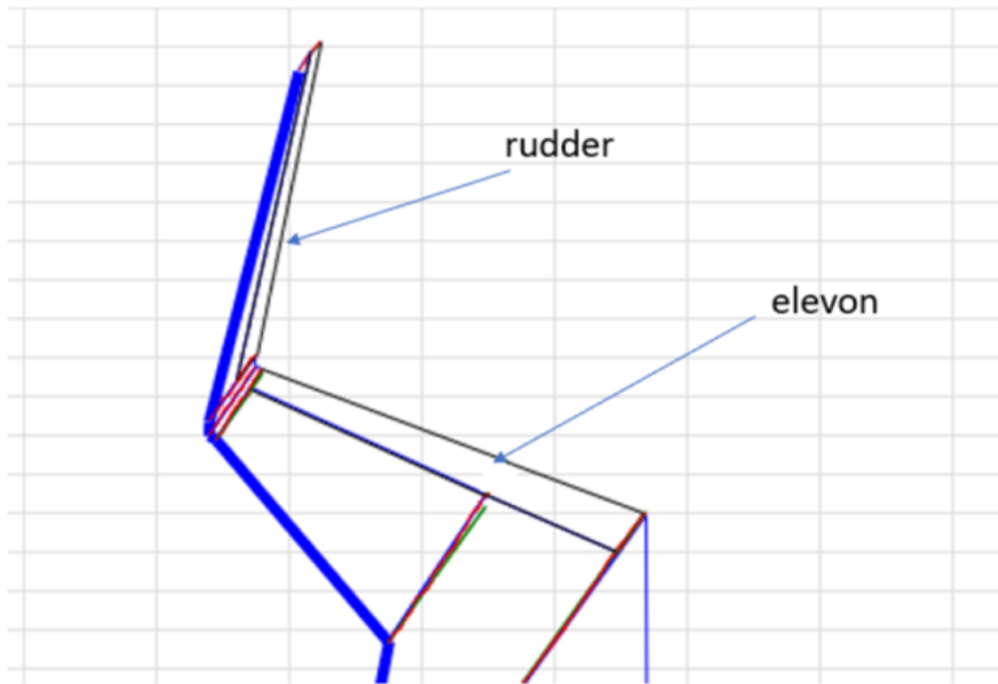


Figure 2.4: Control surface design opted by Tooren[42]

Apart from imposing geometrical constraints like those on maximum span, fuel capacity and even tail height, the constraints provided in context of stability and control are formed on basis of certification requirements enlisted in CS-25 regulations [2]. It was longitudinal control requirement, which proved the critical constraining factor for limiting the safe, feasible range of center of gravity. There were geometrical changes in aircraft, like reduction of sweep angle for outer wing, increase in fin length were expected to increase aerodynamic efficiency. However, in terms of changes or improvements in control authority, this study predicts satisfaction of all control requirements or constraints. It was the hard to satisfy directional control requirements- steady sideslip, One Engine Operative trim condition, which were satisfied by increasing the fin length by 2 m.

The winglet of the aircraft was optimized in a study by Amur[3], where the aim was to improve the aerodynamic efficiency, for which the winglet are primarily used in aircraft. However, this study aimed at multi-objective optimization, therefore stability requirements are to be fulfilled to maximum extent by the winglet design. This study also explores the performance of rudder at maximum deflection. The chord fraction of the rudder is kept at 30%, similar to rudder design opted for the twin fin design by Faggiano[18], considering the rear spar as the constraining factor. The winglet spans over the winglet trunk, with inclusion of 'Kuchemann' tips at ends and appropriate lateral gaps. These features are included also for the reason that analysis is being done in RANS where their effects can be captured through simulation. The rudder parameterization is illustrated in Figure 2.5.

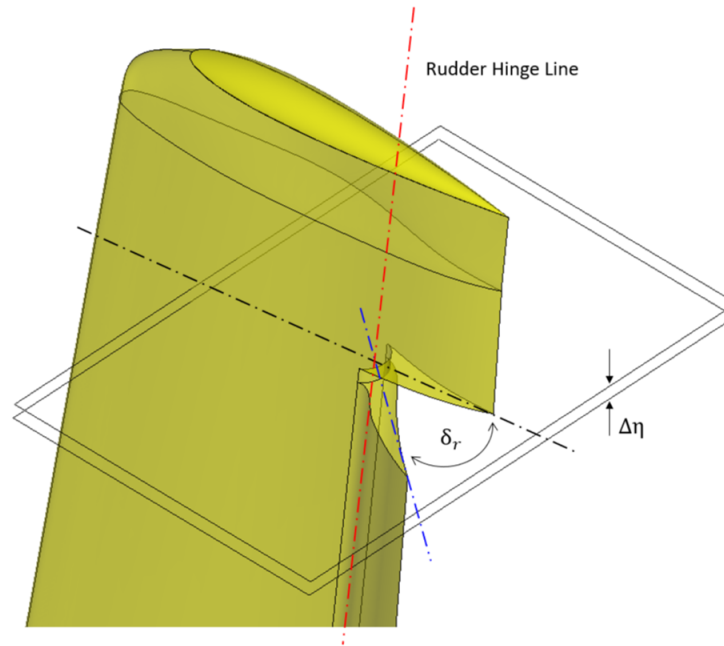


Figure 2.5: Rudder parameterization used by Amur[3] for winglet optimization

The design was optimized by using Oosterom's [33] wing design and a modified version of Horwitz's winglet [23]. In the context of control authority or effectiveness-related changes after optimization, the rudder is predicted to be unable to meet the steady sideslip requirements up to the limiting steady sideslip case of $\beta = 10^\circ$. However, as the sideslip angle increases beyond this point, the aircraft transitions from an unstable to a stable state. This behavior arises from the non-linear response of the yawing moment and side force induced by the winglet with rudder deflection, which reverses the expected trend—shifting from increasing instability toward improved stability. This is addressed by Amur as being caused by "uninvestigated and unexplained flow phenomenon[3]".

The outer wing optimization study by Van Luijk [29] did not involve detailed sizing of the elevons on the outer wing; however, the control surface was included as a constraint during the aerodynamic optimization process. The constraints applied to the control surface dimensions in each iteration were not based on certification requirements for control authority, but rather on geometric limitations—such as restrictions on hinge line placement—or on empirical data from other sources, which suggested that further increases in control surface chord would not lead to significant improvements in control authority. Including the control surface as a constraint in the optimization study limited the achievable aerodynamic efficiency. Specifically, it resulted in a 4.4% reduction in aerodynamic efficiency compared to a case without the control surface constraint.

Nelson[24] studied the aerodynamic effects of winglet/rudder combination in flying V wind tunnel model and the effect of airspeeds on rudder effectiveness, a similar rudder design to Faggiano[18] was used for analysis, a substantial reduction in effectiveness is observed with AoA reaching 20° even more than the decrease in effectiveness with airspeed. As discussed earlier, the handling qualities assessment conducted by Joosten [26] on the control surface design developed by Cappuyns [10] revealed that many certification requirements were not met due to excessive control surface deflections, even with the newly designed control system. Horowitz[23] in his design study of winglet, in accordance with the result, he recommended the study of the limitations in directional stability. Torelli [40] did low-

speed handling quality simulation of Flying V, results indicated that the approach speed, if less than 0.3 Mach might pose control and safety issues. Arjav's[3] performed optimization of winglet design, and a baseline rudder design on the winglet deflected at 30° was found to be insufficient for steady side-slip cases, upto sideslip angle of 10°. The recommendations and results of previous studies on control surfaces for Flying-V presents research opportunities into sizing the control surfaces of an aircraft design as novel as Flying-V.

2.2. Theoretical background for aerodynamic analysis

In this section, descriptions of some important fundamental physical concepts as well as the flow modeling concepts relevant to this thesis are explored. After introducing the concepts which form the theoretical framework of the aerodynamic analysis tool used, the tool itself is introduced, which is the Athena Vortex Lattice (AVL).

2.2.1. Biot-Savart Law

Vortex flow is one of the elementary flow, which can be visualized through a point or through a vortex filament, now this filament can either be a straight line or curve, which generates a flow-field around it. The velocity at any point in the field is quantified through the well-known Biot-Savart Law. In equation 2.1 r is the radius vector to point P, Γ is vorticity strength of the filament and 'dl' is the infinitesimal length vector along the vortex filament length, this is illustrated in 2.6.

$$V = \frac{\Gamma}{4\pi} \int \frac{dl \times r}{|r|^3} \quad (2.1)$$

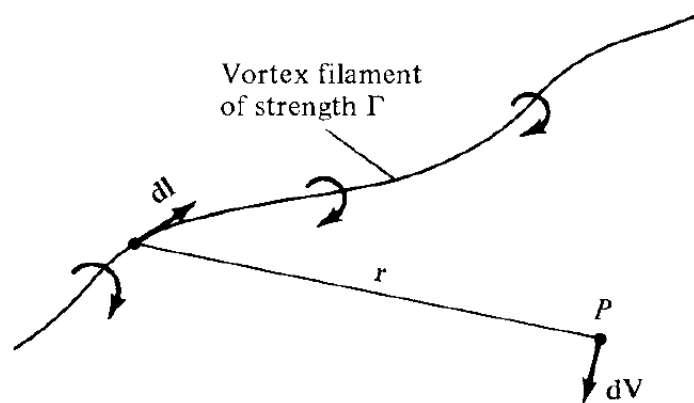


Figure 2.6: Vortex filament induction at a point

Helmholtz was first to introduce vortex filament for analysis of inviscid flow and he proposed two theorems about them [4]: Firstly, "The strength of a vortex filament is constant along its length" and "A vortex line cannot end in a fluid; it must extend to the boundaries of the fluid or form a closed path."

2.2.2. Prandtl Classical Lifting line theory

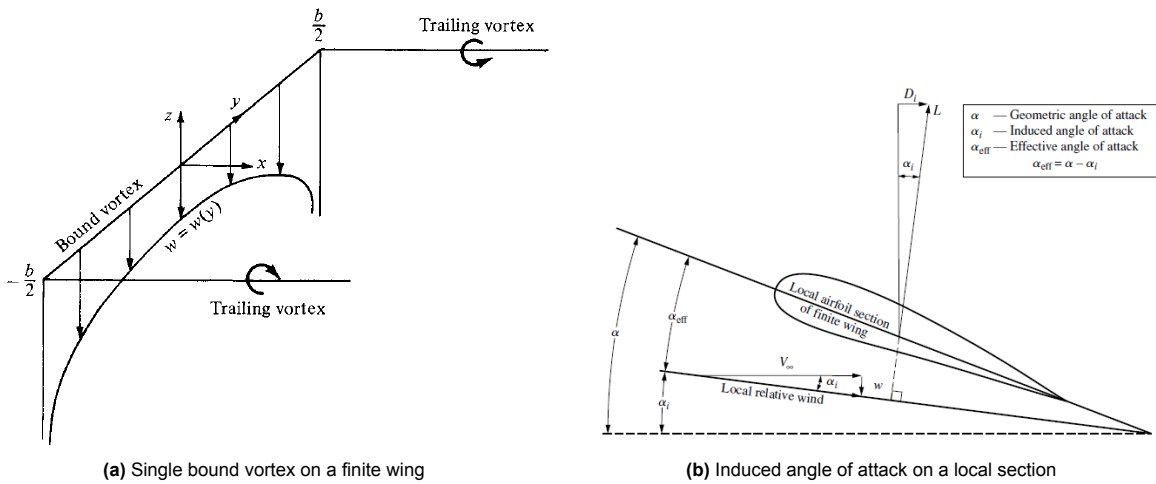


Figure 2.7: Visualization of vortex and induced drag concepts [4]

Ludwig Prandtl with his colleagues came up with this theory in 1911-18[4] to explain the aerodynamic characteristics of a finite wing, by using the "horseshoe vortex filaments". Firstly, the finite wing was replaced by a bound vortex which extended along the wing span, which instead of a free vortex which moves with the flow while this vortex is always with the wing itself 'bound' to it. Now according to Kutta-Joukowski theorem it is known lift depends on circulation of airfoil as follows:

$$L = \rho_{\infty} V_{\infty} \Gamma \tag{2.2}$$

If a singular vortex (in figure 2.7a), which has two trailing semi-infinite vortex (as the filament can't end abruptly in the fluid, Helmholtz theorem), as considered until now if, taken it mathematically leads to infinite downwash at the tips, according to the formula in equation 2.3, where 'w' denotes the downwash and b is the wingspan, whose magnitudes are shown schematically in figure 2.7a.

$$w(y) = -\frac{\Gamma}{4\pi((b/2)^2 - (y)^2)} \tag{2.3}$$

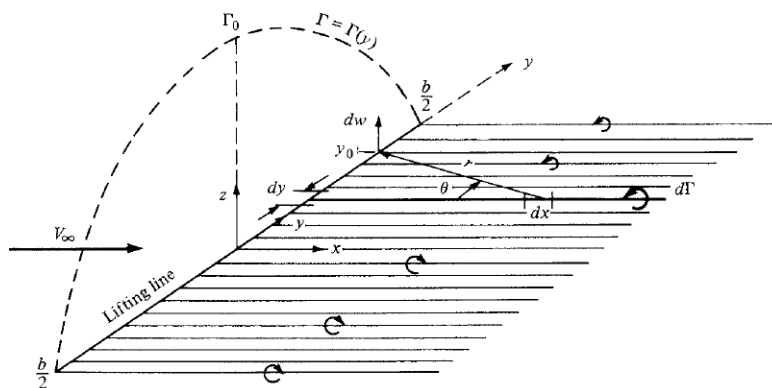


Figure 2.8: Infinite Horseshoe vortices on lifting line [4]

To overcome this conundrum, instead of a single bound vortex, on the lifting line, infinite horse shoe vortices are super-imposed along the lifting line, such that each has an infinitesimal strength of $d\Gamma$ as can be seen in figure 2.8 . The angle of attack equation is formed, which is the fundamental equation of Prandtl's Lifting Line theory (equation 2.4), where geometric angle of attack is represented in terms of effective angle of attack and induced angle of attack. This induced angle of attack is what is responsible for causing induced drag through tilting of the lift vector as can be observed from figure 2.7b.

$$\alpha(y_0) = \frac{\Gamma(y_0)}{\pi V_\infty c(y_0)} + \alpha_{L=0}(y_0) + \frac{1}{4\pi V_\infty} \int_{b/2}^{-b/2} \frac{(d\Gamma/dy)dy}{y - y_0} \quad (2.4)$$

The lift and induced drag generated by the wing both can be calculated by Kutta-Joukowski theorem through application of equation 2.2. Firstly, the lift over the finite wing is mathematically formulated as in equation 2.6.

$$L = \rho_\infty V_\infty \int_{-b/2}^{b/2} \Gamma(y) dy \quad (2.5)$$

$$C_L = \frac{L}{qS} = \frac{2}{V_\infty S} \int_{-b/2}^{b/2} \Gamma(y) dy \quad (2.6)$$

Now for formulating the induced drag, through the vector diagram in figure 2.7b, induced drag per unit span (D'_i) in terms of lift per unit span (L') is formulated as:

$$D'_i = L' \sin \alpha_i \quad (2.7)$$

However if the induced angle of attack is small, $\sin \alpha_i$ can be approximated to α_i , thus the equation becomes:

$$D'_i = L' \alpha_i \quad (2.8)$$

The total induced drag (D_i) is calculated by integrating the equation above over the wingspan, thus final equation for drag and drag coefficient comes out as follows:

$$D_i = \int_{-b/2}^{b/2} L'(y) \alpha_i(y) dy \quad (2.9)$$

$$= \rho_\infty V_\infty \int_{-b/2}^{b/2} \Gamma(y) \alpha_i(y) dy \quad (2.10)$$

Induced drag coefficient is written as:

$$C_{D_i} = \frac{2}{V_\infty S} \int_{-b/2}^{b/2} \Gamma(y) \alpha_i(y) dy \quad (2.11)$$

2.2.3. Vortex Lattice method- VLM

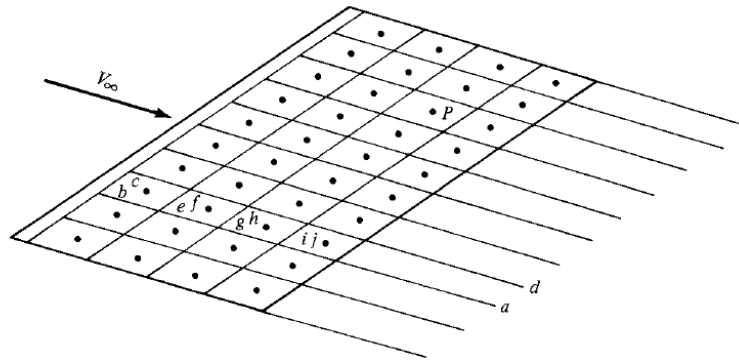


Figure 2.9: Horse-shoe vortex system on a finite wing [4]

Since extensive computational power is accessible, another method of aerodynamic analysis that builds on previously discussed concepts is the Vortex Lattice Method (VLM). Moreover, the lifting line theory does not predict the results for swept wing or straight wing [4], a higher-order method is required. Several horseshoe vortices are superimposed on each other, and this forms a lattice as shown in figure 2.9. To understand the workings of this method, a single horse shoe vortex can be taken, let's take $abcd$ shown in the figure above. The point shown trailing the bound vortex bc is the control point, and usually multiple panels (suppose of length ' l ') are used to define the wing and the bound vortex of horseshoe is placed at $l/4$ along the center line of panel and the control point is placed at $3l/4$. It is at this control point the 'flow tangency' boundary condition is enforced. According to this condition normal velocity component induced at the control point due to horseshoe vortex is zero. Now, multiple horseshoe vortex are now placed to form the vortex lattice system to define the finite wing, each having its own circulation strength. After considering the superposition of vortices, it can be seen that strength varies spanwise, and chord wise along the wing, but for trailing wake the vortices vary in strength along the span of wing as there are no vortices used to model wake here parallel to direction of span of wing. Finally, considering all the control points, and using Biot-Savart law to measure velocity at control point induced due to all the horseshoe vortices, and normal component must be zero. This forms a system of equations, which when solved leads to value of strengths of all the vortices. These values and then are used to measure the required forces and moment.

For control surfaces, the flow tangency condition is applied by rotating the normal vector (n_{0_i}) at control surface depending on the deflection of control surface, defined by δ_l (where l is control index varies from 1 to N), instead of using the control deflection angle (δ_e or δ_a), done about hinge vector (\hat{h}_{l_i}), as shown in figure 2.10. The equation of normal vector (n_i) is shown in equation 2.12

$$n_i(\delta_l) = n_{0_i} + \sum_{l=1}^N n_{l_i} \delta_l \quad (2.12)$$

where n_{l_i} is expressed mathematically as

$$n_{l_i} = \frac{\partial n_i}{\partial \delta_l} = g_l \hat{h}_{l_i} \times n_{0_i} \quad (2.13)$$

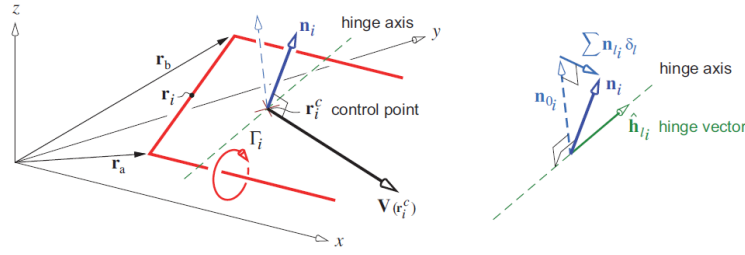


Figure 2.10: Flow tangency condition at a control point- influenced by rotation of vector by deflection[15]

Flow tangency boundary condition is imposed at the control point, as shown above for a control point on control surface, using Biot-Savart law and considering the N_v horseshoe vortex system, where U is aircraft velocity and Ω is the rotation rate and the free stream velocity- V_∞ , mathematically the equation for imposing this condition can be written as follows:

$$\left(\sum_{i=1}^{N_v} \Gamma_i \hat{V}_i(r_i^c) - (U + \Omega \times r_i^c) \right) \cdot n_{0_i} + \sum_{l=1}^{N_l} V_\infty \hat{x} \cdot n_{l_i} \cdot \delta_l = 0 \tag{2.14}$$

2.2.4. Trefftz Plane-far field analysis

In lifting line theory, the finite wing is replaced by single lifting line and the variation of vortex strength along the stream wise direction is not considered, so if a thin trailing vortex sheet is considered, then through the method of Trefftz plane analysis, where to compute forces on the body analysis is done on far downstream plane and it is also termed as far-field analysis.

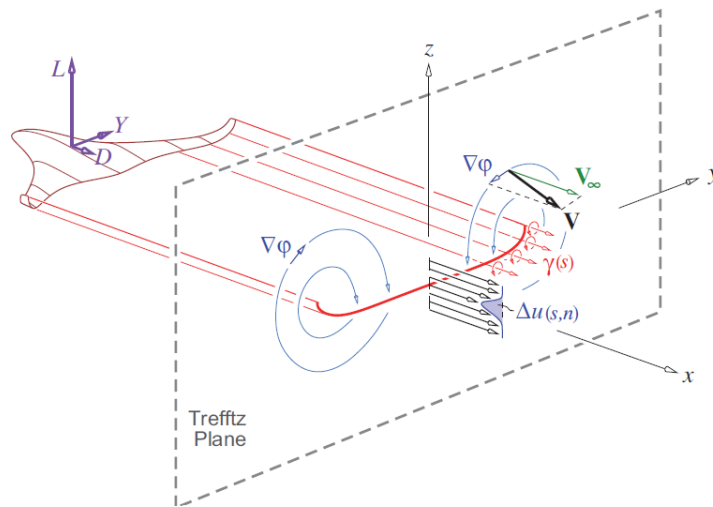


Figure 2.11: Trefftz plane analysis for induced drag, with focus on perturbations caused in the Trefftz plane [15]

To summarize how drag is calculated mathematically, integral momentum is applied in the x-direction, and the Trefftz plane is sufficiently far-away that except for the perturbations downstream in the Trefftz plane, everywhere else the perturbations are zero. Perturbation velocity is denoted by $\nabla\phi$ and u' , v' and w' are x,y and z component of perturbation velocity.

$$\nabla\phi^2 = v'^2 + u'^2 + w'^2 \tag{2.15}$$

Moreover, it is further assumed that perturbations along x-direction (free-stream flow direction) dies away, and perturbation along x-direction much lower than perturbation in yz plane[15]

$$u'^2 \ll v'^2 + w'^2 \quad (2.16)$$

The final mathematical equation for induced drag via this method lead to equation 2.17.

$$D_i = \frac{1}{2}\rho \int \int_{S_T} (v'^2 + w'^2) dS \quad (2.17)$$

So only perturbations in the yz plane, caused by the trailing vortices is considered for drag calculation as seen in equation above, and it can further be observed that the induced drag is caused because kinetic energy is transferred into cross flow (in the yz plane, via trailing vortices), and it can also thus be concluded that induced drag is countered by the aircraft's thrust and thus propulsive energy is lost to induced drag.

3

Methodology

This chapter mainly deals with description of tools used for aerodynamic analysis tool required for control surface sizing, then various certification requirements pertinent to the control surfaces to be sized are enlisted and mathematical equations involved in the respective maneuvers are given which use the stability and control derivatives derived as a result of the aerodynamic analysis. The final section deals with the method to size the control surfaces. This section includes the reasoning behind the chosen objective function when optimization of the control surface is pursued, with explanation of the optimization algorithm and procedure adopted.

3.1. Athena Vortex Lattice- AVL

The analysis of control authority of a control surface requires the aerodynamic forces and moment results in the required conditions, to obtain these results a tool to simulate the required condition is needed which can be aptly chosen according to the level of detail and accuracy required. Since the main objective is to search for the most optimized design of control surface with sufficient control authority, this leads to a lot of design iterations to be run at predefined aerodynamic parameters(density, speed etc.), during the optimization, a relatively quick and simpler numerical method is required for which Vortex Lattice Method can be considered appropriate. Although higher order methods such as RANS and LES offer more accurate and detailed solutions and also capture turbulence in the flow at smaller scales, these methods are based on solving modified forms of Navier-Stokes equations , VLM uses a system of equations as discussed in Section 2.2.3, and provides a comparatively faster solution.

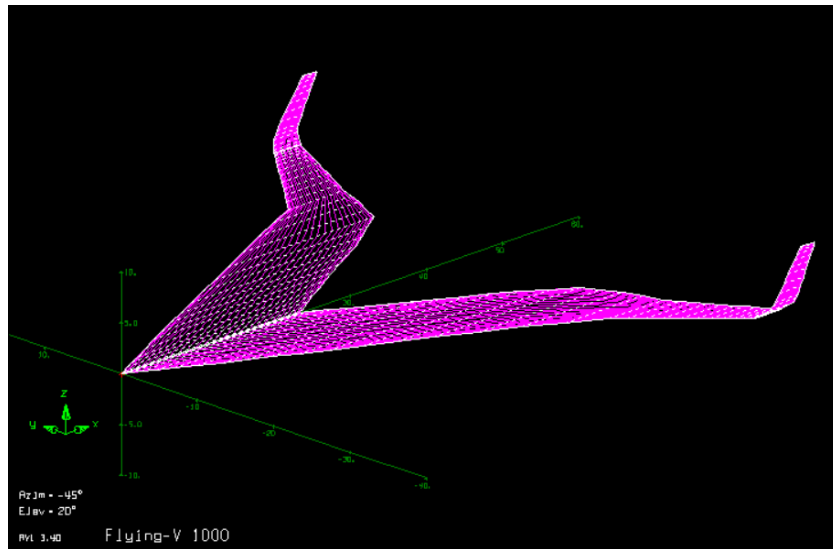


Figure 3.1: Geometry of Flying-V analyzed in AVL

The software tool used here for analysis is AVL- Athena Vortex Lattice- which was written in 1988 by Harold Youngren, build upon the previous work of other contributors, notably Lamar and L. Miranda (VORLAX)[14]. In AVL, compressibility is treated using Prandtl-Glauert Transformation, as explained in its user guide [14], this remains valid for mach number below 0.6. In this study, almost all aerodynamic analysis is conducted in range of 0.2 to 0.25, so reasonable results are to be expected. This software conducts analysis on a defined geometry, which is formed as an '.avl' file, and the states and parameters can be set in the command interface or input as '.run' file. The geometry for flying V here is defined by using spanwise sections, which include leading edge coordinates and chord at each section and the defining of vortex spacing. The vortex spacing for the wing consists of 30 vortices for half-wingspan, using cosine spacing in both the spanwise and chord wise directions, resulting in a total of 60 vortices across the full span. Similarly, as both winglets are defined as separate surfaces in the .avl geometry file, their vortex spacing is specified as follows: 30 chord wise vortices and 15-vortices spanwise. The use of cosine spacing is intended to increase the concentration of vortices near the winglet tips and the wing-winglet junction. Additionally, chord wise cosine spacing ensures higher vortex density at the leading and trailing edges of the wing and winglets. The final geometry of the FV-1000 that was used can be seen in figure 3.1. The geometry of FV-1000 used in this study is the one provided by Laar[28]. The avl command interface does provide the option to conduct analysis through sweep of angles, like angles of attack(α), but another way to automate the varying flight parameters and states is by using the 'AVLWrapper' package in python [37].

3.2. Certification requirements for control authority

The control surfaces of a civil aircraft need to satisfy specific certification requirements, which are laid down by governing authorities. The regulations of interest in this study are from Certification Specifications and Acceptable Means of Compliance for Large Aeroplanes- (CS-25- 28th Amendment) [2], which are laid down by European union Aviation Safety Agency. The critical criteria for each control surface is identified and chosen, so feasibility of a particular control surface layout or design can be evaluated, these were already listed in Tooren[42], in this study the surfaces must satisfy these requirements to prove their utility. The mathematical equations to define each criteria is taken from Kay[27], where defi-

dition of many such requirements or performance considerations are compiled with respective sources, but the ones relevant to the control surface whose designs are under consideration (aileron, elevator and rudder).

The criteria are enlisted in succeeding sections with inclusion of flight conditions at which control surface need to perform (velocity, angle of attack) and also the center of gravity position is defined which is considered the most limiting case.

3.2.1. Longitudinal Trim

The aircraft should be able to longitudinally trim itself for a level flight, which can be done at all operational speed, to be more precise according to CS-25[2], 28th amendment regulation, "Level flight at any speed from $1.3 V_{SR1}$, to V_{MO}/M_{MO} ". Based on the fact that net vertical force and moment being zero at longitudinal trim, equations below describe the mathematical relation among the angle of attack, elevator's deflection angle and the relevant aerodynamic coefficients, these are taken from Kay[27], where in turn these are based on equations from Etkin[17] :

$$C_{Ltrim} = \frac{W}{qS} = C_{L0} + C_{L\alpha} \alpha_{trim} + C_{L\delta_e} \delta_{e_{trim}} \quad (3.1)$$

$$C_m = 0 = C_{m0} + C_{m\alpha} \alpha_{trim} + C_{m\delta_e} \delta_{e_{trim}} \quad (3.2)$$

From 3.1 we can get α_{trim} ,

$$\alpha_{trim} = \frac{C_{Ltrim} - C_{L0} - C_{L\delta_e} \delta_{e_{trim}}}{C_{L\alpha}} \quad (3.3)$$

Putting α_{trim} 's expression into 3.2, and also with help of the fact that,

$$\frac{C_{m\alpha}}{C_{l\alpha}} = \frac{dC_m}{dC_L} \quad (3.4)$$

following equation for $\delta_{e_{trim}}$ is obtained:

$$\delta_{e_{trim}} = \frac{C_{m0} + \frac{dC_m}{dC_L} (C_{Ltrim} - C_{L0})}{-C_{m\delta_e} + \frac{dC_m}{dC_L} C_{L\delta_e}}$$

As $C_{Ltrim} = W/qS$ from equation 3.1, so now equation above becomes:

$$\delta_{e_{trim}} = \frac{C_{m0} + \frac{dC_m}{dC_L} \left(\frac{W}{qS} - C_{L0} \right)}{-C_{m\delta_e} + \frac{dC_m}{dC_L} C_{L\delta_e}} \quad (3.5)$$

The most limiting or constraining condition at which aircraft needs to be longitudinally trimmed is at Maximum Landing Weight (MLW), with C.G. being at most forward position, with flight speed at approach speed (V_{app}).

3.2.2. Lateral control: Time-to-bank

One requirement which is crucial for an aileron design to fulfill is the 'Time-to-bank' which puts requirements on the aircraft to be able to have enough control authority or capability to perform a banking maneuver in a specified time-limit. According to CS 25.147 (AMC 25.147(f)) [2], the aircraft must be able to roll from a steady 30° banked position through about 60 degrees to a banked 30° in opposite direction in or under 7 seconds. The most constraining condition is at approach speed, while weighing

at Maximum Landing Weight (MLW), with the CG being at aft most position[42]. Now, for the mathematical expression to assess the ability to execute this rolling motion, deflection angle is kept constant here, following are the required expressions:

$$\dot{\phi} = p \quad (3.6)$$

$$\dot{p} = \frac{qSb}{I_{XX}} \left[C_{l_{\delta_a}} \delta_a + (C_{l_p} p) \left(\frac{b}{2V} \right) \right] \quad (3.7)$$

The equation for bank angle as a function of time which is used to finally test if required bank angles are reached within certified times or not, is found by integration of roll rate equation, with aileron deflection assumed constant, this equation is put forth by Kay[27]:

$$\phi(t) = -\frac{2V}{b} \frac{C_{l_{\delta_a}} \delta_a}{C_{l_p}} \left[t + \frac{1}{L_p} (1 - e^{L_p C_{l_p} t}) \right] \quad (3.8)$$

Roll mode time constant is defined as $-L_p^{-1}$, whose expression is the following:

$$L_p = \frac{qSb^2}{2VI_{XX}} C_{l_p}$$

3.2.3. Steady Sideslip

Aircraft requires sufficient roll and yaw control power to be able to keep steady sideslip, and there are certain guidelines by certification bodies which define the conditions for these requirements. The crosswind component at which steady sideslip has to be maintained is based on the maximum crosswind velocity defined in CS 25.237[2], which states it should be at least 37 km/h (or 20 knots) or 0.2 times stall speed, whichever is larger, but this crosswind velocity must not exceed 25 knots or 46 Km/h-(12.86 m/s).

The rudder and aileron both are used to maintain this steady sideslip, and the bank angle should not exceed 5° [27]. The limit on aileron deflection is 25° [42] and rudder the maximum deflection is capped at 30° [32].

The most limiting condition or critical flight condition for steady sideslip is at MTOW at minimum control speed [42]. While checking the feasibility of a rudder-aileron combination for steady sideslip both extremes of CG position-forward and aft are considered. The mathematical formulation[17],[27] to express the unknown angles (δ_r , δ_a and ϕ) is derived from first forming the equations for side force, yawing and rolling moment coefficient for trim :

$$C_{Y_\beta} \beta + \left(\frac{W}{qS} \right) \cos(\gamma) \phi + C_{Y_{\delta_r}} \delta_r + C_{Y_{\delta_a}} \delta_a = 0 \quad (3.9)$$

$$C_{n_\beta} \beta + C_{n_{\delta_r}} \delta_r + C_{n_{\delta_a}} \delta_a = 0 \quad (3.10)$$

$$C_{l_\beta} \beta + C_{l_{\delta_r}} \delta_r + C_{l_{\delta_a}} \delta_a = 0 \quad (3.11)$$

Solving 3.10 and 3.11 together provides the rudder angle (δ_r) and aileron angle (δ_a). These values are put into equation 3.9 to find the required bank angle.

$$\delta_r = \beta \frac{-C_{n_{\delta_a}} C_{l_\beta} + C_{l_{\delta_a}} C_{n_\beta}}{C_{l_{\delta_r}} C_{n_{\delta_a}} - C_{n_{\delta_r}} C_{l_{\delta_a}}} \quad (3.12)$$

$$\delta_a = \beta \frac{C_{n_{\delta_r}} C_{l_\beta} - C_{l_{\delta_r}} C_{n_\beta}}{C_{l_{\delta_r}} C_{n_{\delta_a}} - C_{n_{\delta_r}} C_{l_{\delta_a}}} \quad (3.13)$$

$$\phi = - \frac{C_{y_\beta} \beta + C_{y_{\delta_r}} \delta_r + C_{y_{\delta_a}} \delta_a}{\frac{W}{qS} \cos \gamma} \quad (3.14)$$

3.2.4. One- Engine Inoperative (OEI) trim

In case that one-engine fails, an aircraft should have enough roll and yaw control authority to achieve trim under such conditions. This is thus achieved by operating the rudders and ailerons together, and this must be done at the most limiting condition of being at minimum control speed (V_{mc}), with weight being Maximum Take-Off Weight (MTOW) [42]. Similarly to steady sideslip, while checking a control surface configuration for OEI trim requirement, both forward and aft CG can be tested. Before stating the mathematical expressions, the side force and rolling effects of the asymmetrical thrust as well as the windmilling drag of the inoperative engine of OEI condition is ignored, and only the significant induced yawing moment is considered for countering by control surfaces, and this yawing moment coefficient is evaluated as follows [42]:

$$C_{n_{OEI}} = \frac{N_{OEI}}{qS} = \frac{-0.5 T_{TOY_{eng}}}{qS} \quad (3.15)$$

Now similar to steady sideslip with the required modification we form the equations for trim similar to what was done by Kay [27], but here sideslip angle is ignored or assumed to be zero, as was done by Faggiano [18], while the satisfying requirement of OEI was framed although aileron deflections were ignored in that study, which leads to following equation:

$$C_Y = 0 = \frac{W}{qS} \cos(\gamma) \phi + C_{Y_{\delta_r}} \delta_r + C_{Y_{\delta_a}} \delta_a \quad (3.16)$$

$$C_{l_{\delta_r}} \delta_r + C_{l_{\delta_a}} \delta_a = 0 = C_l \quad (3.17)$$

$$C_{n_{\delta_r}} \delta_r + C_{n_{\delta_a}} \delta_a + C_{n_{OEI}} = 0 = C_n \quad (3.18)$$

The equations for bank angle and control surface deflections can be derived using the three trim equations above.

3.2.5. Longitudinal- Pull-up Maneuver

The aircraft should be able to carry out the longitudinal pull up Maneuver at the required load factor (n) as stated in the airworthiness regulations. As stated in Section 6- Acceptable Means of Compliance - Flight Test Program: General Controllability and Manoeuvrability in CS-25 [2], a load factor of 1.3 g is required; the limiting case for executing this maneuver is at approach speed with aircraft weighing at Maximum Landing Weight (MLW), C.G. at the most forward position. [10] [42]. The effect of this maneuver on control surface deflection and angle of attack of the aircraft, in terms of change in these values, can be determined mathematically as shown below which was derived by Kay [27].

The pulling up maneuver constitutes the generation of additional lift (ΔC_L) and pitch rate, another point to note is this motion begins from 1-g trimmed flight, these two terms can be expressed as following:

$$\Delta C_L = \frac{\Delta L}{qS} = \frac{(n-1)W}{qS} \quad (3.19)$$

pitch rate is expressed in a non-dimensionalized manner(\hat{q}):

$$\hat{q} = \frac{(n-1)\bar{c}g}{2V^2} \quad (3.20)$$

The additional lift coefficient(ΔC_L) can be expressed in terms of change in angle of attack or elevator deflection with help of stability and control derivatives(equation 3.21) , same for change in pitching moment coefficient(ΔC_m)(eq. 3.22), but as flight needs to trimmed , $\Delta C_m = 0$,

$$\Delta C_L = C_{L_\alpha} \Delta\alpha + C_{L_q} \hat{q} + C_{L_{\delta_e}} \Delta\delta_e \quad (3.21)$$

$$\Delta C_m = 0 = C_{m_\alpha} \Delta\alpha + C_{m_q} \hat{q} + C_{m_{\delta_e}} \Delta\delta_e \quad (3.22)$$

Using the values expressed in equations 3.19 and 3.20, substitute them in equations 3.21 and 3.22, which can then be solved for the two unknown quantity elevator deflection angle($\Delta\delta_e$) and change in angle of attack($\Delta\alpha$) which can help in confirming whether they are crossing the design limitations.

3.2.6. Take-off rotation speed:

The take-off rotation speed is defined as speed at which enough dynamic pressure exists that the wheel just comes off the ground, hence the aircraft rotates as explained in Kay[27]. It is the elevator or elevon which provides the required moment which helps in lifting the nose-wheel of the ground. Thus the moment due to weight of aircraft is to be countered by aerodynamically derived moment due to deflection of elevator, which in case of Flying-V is deflection upwards or negative. The angle of attack while the aircraft is accelerating on ground is taken based on strut lengths of nose and main landing gear, which if based on study by Bourget[9], comes out to be -3.92° . The elevator would be deflected upwards to the maximum limit based on Tooren's study[42]. The formula for calculating the rotation speed is presented as equation 3.23[42].

$$V_R = \sqrt{\frac{W(x_{cg} - x_{mlg})}{-\rho\bar{c}S C_{m_{mlg}}}} \quad (3.23)$$

The position of landing gear- x_{mlg} is taken from the study by Bourget[9]. The term- ' $C_{m_{mlg}}$ ' is the coefficient of moment about the main landing gear. The requirement for this speed as stated in CS-25 .107 [2] is that this speed is less than minimum take-off safety speed- ($V_{2_{min}}$) plus the speed gained before reaching the height of 11 m . However, when Tooren imposed the constraint on rotation speed, it was framed as $V_R < V_{2_{min}} - 5$, which means a more conservative constraint was put forth.

3.2.7. High Angle of attack departure: Lateral Control Departure Parameter (LCDP)

& $C_{n_{\beta_{DYN}}}$

Apart from maneuvers and trim cases required to be executed to test the control authority of the surfaces, there are other parameters to test departure tendency of the aircraft, at high angle of attacks. The one under consideration here is the lateral Control Departure Parameter- 'LCDP'. As stated by Kay[27], LCDP indicates the spin resistant capability of aircraft [11] and if the configuration is not prone to departure induced by aileron deflection at high AoA [25].

$$LCDP = C_{n_\beta} - \frac{C_{n_{\delta A}}}{C_{l_{\delta A}}} C_{l_\beta} \quad (3.24)$$

A positive value of this parameter (LCDP>0), indicates the design being resistant to departure tendencies of spin and aileron induced departure. Evaluating this parameter at the most limiting angle of attack is the appropriate step to check this parameter, where it must be positive. This angle of attack is set to be limited to 20 degrees, as imposed by Tooren[42], as pitch break is expected to occur when AoA starts increasing above 20°.

The other parameter of interest at high angle of attack, although not related to control authority, is the " $C_{n_{\beta DYN}}$ ". This parameter gives indication of open loop directional stability of aircraft. Aircraft with positive value of this parameter for high angle of attack, which here is taken as 20 degrees [42], the aircraft is predicted to be resistant to yaw departure. The equation for calculating this parameter is as follows:

$$C_{n_{\beta DYN}} = C_{n_{\beta}} \cos \alpha - \frac{I_{zz}}{T_{xx}} C_{l_{\beta}} \sin \alpha \quad (3.25)$$

All the requirements stated till now are summarized in table 3.1. The values of limitations on deflections of elevator, aileron and rudder are stated in later sections as well, where these requirements are to be checked as part of the sizing procedure or to test the optimized designs against these requirements.

Table 3.1: Certification requirements - tabulated

Certification requirements	Flight condition	Constraint
Longitudinal trim	Forward CG & approach speed, MLW	$\delta_e < \delta_{e,max}; \alpha < \alpha_{max}$
Longitudinal maneuver pull-up (1.3 g)	Forward CG & approach speed, MLW	$\delta_{e,final} < \delta_{e,max}; \alpha_{final} < \alpha_{max}$
Time to bank	Aft CG & approach speed	$\phi > 60^\circ$
Steady sideslip	V_{mc} , MTOW	$\delta_a < \delta_{a,max}; \delta_r < \delta_{r,max}; \phi < \phi_{lim}$
OEI trim	V_{mc} , MTOW	$\delta_a < \delta_{a,max}; \delta_r < \delta_{r,max}; \phi < \phi_{lim}$
Take-off rotation speed (V_R)	$\alpha = -3.92^\circ; \delta_e = -25^\circ$, forward CG, MTOW	-
$C_{n_{\beta DYN}}$ & LCDP	$\alpha = 20^\circ$	LCDP > 0 & $C_{n_{\beta DYN}} > 0$

3.3. Initial optimization- objective function-selection

The sizing of control surfaces- aileron, elevator and rudder are subjects of interests. The control surfaces designed must satisfy the constraints required which can be derived from the requirements explained in section 3.2. One option to find a feasible design is to go through several iterations of control surface design and check which one satisfies the constraints. However, if the sample pool of designs is too large, an optimization algorithm with an appropriately chosen objective function and constraints might be the more efficient option.

Therefore, in this study, instead of testing a set of layouts for the control surface, a step-by-step procedure is chosen to design control surfaces. The optimization procedure requires an appropriate objective function to be minimized. To select the apt value to be minimized, two coefficients- " C_D " and " C_{HM} " are first used to optimize the control surface design. The control surface chosen to be optimized to test the objective functions is the elevator, at longitudinal trim. To simplify the parameterization of control surface, the elevator span is kept as the whole trailing edge of the outer wing. This span extends from the outermost trailing edge kink in the wing (at y=21 m) to just before the wing transitions into winglet(at y=30.6 m), similar to the control surface span used by Cappuyns[10].The optimization problem can be

expressed in mathematical terms as following:

$$\text{Minimize } F_{obj}(x); \quad (3.26)$$

Subject to these constraints at longitudinal trim

$$\delta_e < 25 \quad (3.27)$$

$$\alpha < 20 \quad (3.28)$$

The F_{obj} takes the value of drag coefficient(C_D) and hinge moment coefficient(C_{HM}), so that results are to be observed and a single objective function is eventually selected. Minimizing drag is always integral to designing a subsonic-large civilian aircraft, as minimizing the drag leads to less consumption of fuel, which is a priority while designing such a civil aircraft. Another objective function which is considered is the hinge moment coefficient because it is critical to calculate the actuation power required to operate the control surface. As explained by Denieul[13], this actuation power required for a control surface can be approximated by a quantity called corner power(P_{CP}) (equation 3.29), which is actuation power required at the stall load at maximum deflection rate. Corner power(P_{CP}) is calculated by maximum hinge-moment(HM_{max}) and maximum deflection rate($\dot{\delta}_{max}$). However, actuation power(P_{act}) is approximated as shown in equation 3.30[20]

$$P_{CP} = HM_{max} \times \dot{\delta}_{max} \quad (3.29)$$

$$P_{act} \approx 0.85P_{CP} \quad (3.30)$$

In some mass estimation models, the maximum hinge moment is used as an input to calculate the actuator's mass.[39][13]. If the deflection rate is assumed to be constant for any maneuver involving a control surface, the hinge moment under the most critical flight conditions, in terms of control authority, can be minimized as an objective function(F_{obj}). While the mass estimation model uses the maximum hinge moment as an input, optimization for minimizing the C_{HM} , eventually leads to minimizing the hinge moment for all conditions(i.e. across the range of dynamic pressure), which means that the maximum hinge moment(HM_{max}) reduces as well. Thus, a decrease in HM_{max} can be expected, which in turn reduces the required actuator power (Equation 3.30) and actuator mass (as predicted by certain mass estimation models). This approach reduces the required actuator power and mass while ensuring that the control surface design complies with the certification requirements.

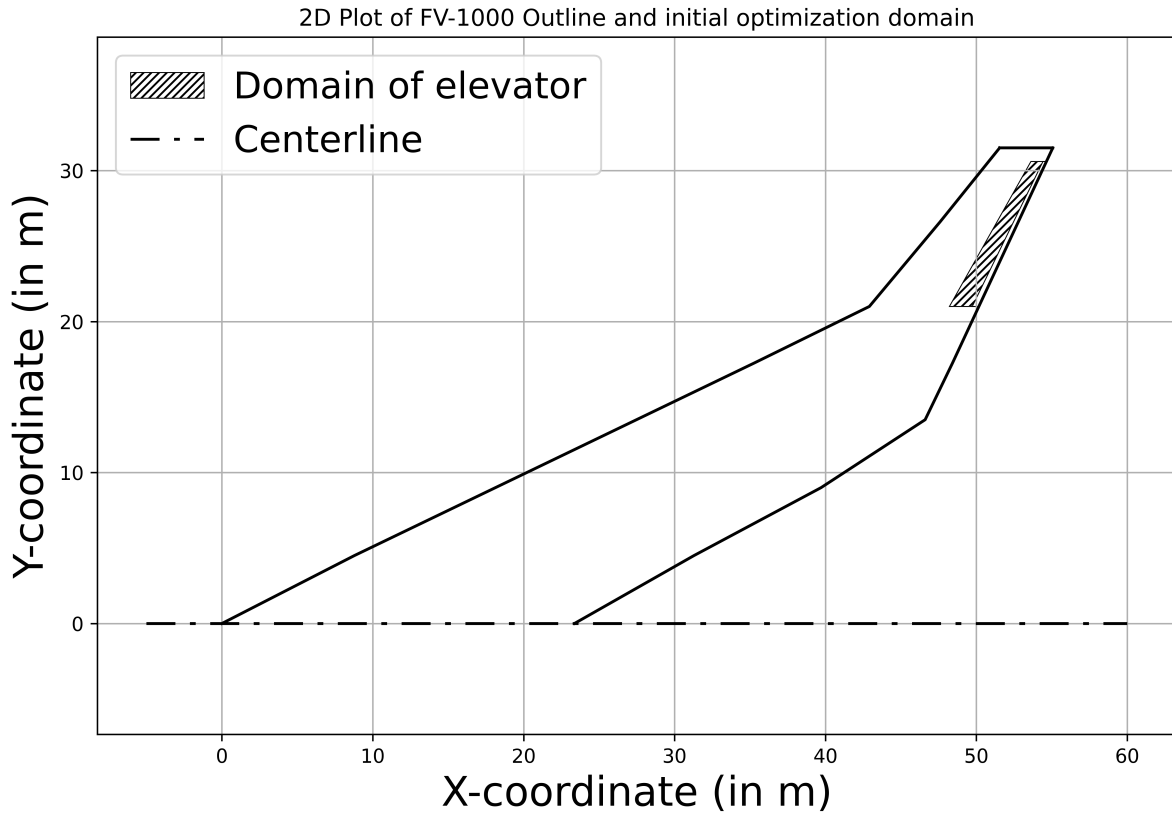


Figure 3.2: Elevator's area of domain used for initial optimization trial

The domain over which this initial optimization is conducted, over the outer wing of FV-1000, the lower bound set on chord percentage (chord percentage at which the control surface hinge line is placed) is set at 73.13% of chord. This is derived from the scaled layout of FV-1000 provided by Oosterom[33], it can be seen in figure 3.2 as a shaded area. The limit for chord comes from the fuel tank as presented in layout by Oosterom[33]. The study by Van Der Tooren[42], place the rear spar at 60% of the chord, drawn perpendicular to the leading edge of the outer wing. This chord percentage translates to 69.18% in streamwise direction (which is the way it is defined in AVL). Therefore, a more restricting bound is chosen for this study, choosing 73.13% instead of 69.18%. There are two ways in which this optimization can be done, apart from trying objective functions- C_{HM} & C_D , it is either allowing different hinge line chord fractions at the inboard(in_c) and outboard(out_c) ends of the control surface (elevator), or keeping a constant chord fraction of hinge line of the elevator at both ends. Mathematically this can be framed as:

$$x = [inboard\ end\ chord\ fraction, outboard\ end\ chord\ fraction] \quad (3.31)$$

OR

$$x = [Constant\ chord\ fraction] \quad (3.31)$$

The optimization algorithm used here is CMA-ES (Covariance Matrix Adaptation Evolution Strategy), which is a stochastic, evolutionary based optimization algorithm, and can be applied in many type of cases as discussed in Mkhoyan et al.[31][36][16]. This algorithm has good convergence behaviour as well, although not a surety, but it does converge on many functions[21]. Therefore, for optimization for control surface design, this algorithm is utilized. To integrate AVL aerodynamic analysis and opti-

mizer to optimize the objective function(in this case, which are C_{HM} and C_D), Python is used as the programming language. In further detail, the avlwrapper package[37] is utilized in conjunction with the cma package [22] for optimization.

For the constant-chord fraction and different-chord fraction-based optimization, results are tabulated in table 3.2 and the figures 3.3a & 3.3b display the optimized control surfaces respectively.

Case	Objective Function	Design Vector	Elevator Deflection [°]	AoA [°]	C_D	C_{HM}
Different chord fraction at ends	C_{HM}	[0.8088, 0.7984]	24.97	17.97	0.04881	0.000235
Different chord fraction at ends	C_D	[0.7314, 0.7376]	21.91	18.00	0.04875	0.000263
Constant chord fraction at both ends	C_{HM}	[0.791, 0.791]	24.20	17.98	0.04879	0.000245
Constant chord fraction at both ends	C_D	[0.7408, 0.7408]	22.14	17.99	0.04875	0.000264
					% Improvement in C_D for constant-chord	0.12%
					% Improvement in C_{HM} for constant-chord	7.19%

Table 3.2: Results of initial optimization cases

The optimization results with C_D as an objective function can be observed from the results tabulated in Table 3.2. The case where the design variables are the different chord fractions (equation 3.31), resulting fractions for both ends of elevator are 73.14%-inboard end and 73.76%-outboard end (in figure 3.3b). The case of constant chord fraction at both ends, as formulated in design variable (equation 3.3), the resulting optimized design is 74.08% (in figure 3.3a). The chord fractions for both cases are very close to the lower bound (73.13%). This means optimization with the objective of minimizing drag for designing a control surface, which in this case is elevator, leads to a design which is control surface with chord as large as possible. This increasing of size by shifting hinge line as forward as possible is the result of aiming for a design which deflects to a lesser or minimum angle.

The resulting optimization designs with C_{HM} as objective function show a different trend. The optimization case where chord fractions for elevator are with different chord fraction-ends (equation 3.31)-results are 80.88% (inboard end) and 79.84% (outboard end) (in figure 3.3b). The optimization case when constant chord fraction is enforced at both ends of elevator (equation 3.3) result is hingeline at 79.1% (as illustrated in figure 3.3a). The results for both cases indicate the same thing, optimizer tries to minimize the chord of control surface, but only to the extent that no constraints are violated (equations 3.28) and C_{HM} can be minimized.

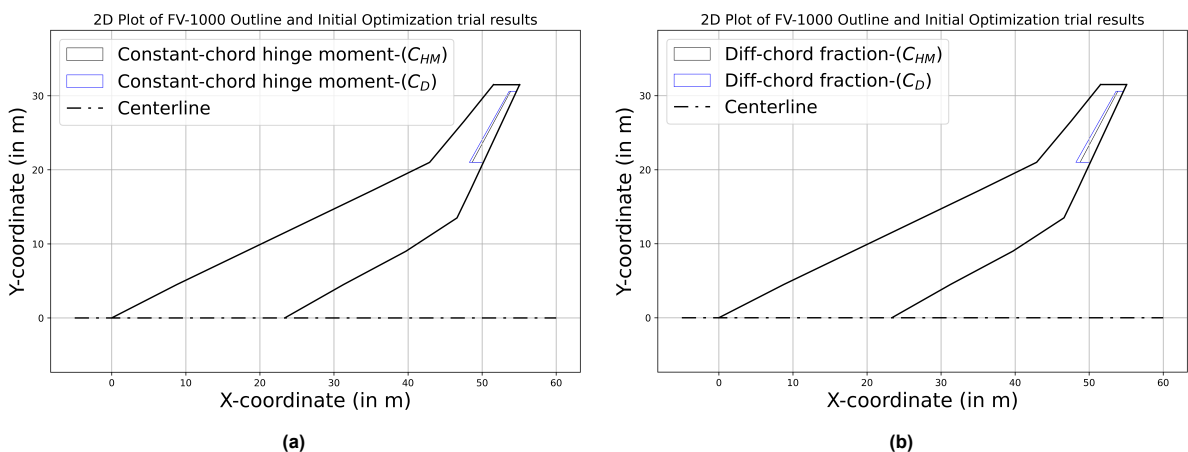


Figure 3.3: Optimized elevators-results of initial optimization:a) Constant chord fraction ;b) Different chord fraction

Based on the overall results, tabulated in Table 3.2 the comparison of both cases-constant chord

fraction-based optimization and case where design variables allow different chord fractions at both ends, an important observation is made. The second case offers the optimizer flexibility to choose vastly different chord fractions for both ends, but the convergence leads to a result for the second case has fractions just different from each other by at most 1%. It can be concluded that including different variables in the design vector for the inboard end chord fraction and outboard end chord fraction does not offer much different or improved results. Therefore, all the sizing and optimizing of control surfaces is to be done by opting for constant chord fraction at both ends for the control surface.

This decision can also be supported by the fact that different chord fractions might pose structural difficulties compared to designs with constant chord fraction. In particular, different chord fractions can require the spars to be curved instead of straight spars[38], which are structurally simple.

To finalize on the objective function, the optimized design results based on minimizing the hinge moment coefficient (C_{HM}) and the drag coefficient (C_D) are compared. When the drag coefficient of both cases are compared, for the optimized design based on C_D only an improvement of 0.12% is observed compared to the optimized design based on C_{HM} . However, the optimized design based on C_{HM} , shows 7.19% reduction in the hinge moment coefficient compared to the optimized design based on C_D , noticeably bigger than improvement in C_D . Optimizing with C_{HM} offers a more compact design, that is, the hinge line is shifted aft, and drag coefficient does not differ much from the optimized design based on C_D , while there is significant improvement in hinge moment coefficient. In summary, opting for C_{HM} as objective function leads to a more compact design, thus saving space, and lesser C_{HM} potentially reduces actuator mass, while the resulting design still satisfies the imposed constraints.

3.4. Method adopted for control surfaces

The sizing of three control surfaces is aimed: aileron, elevator and rudder. These three are to be tackled first because they are the main control surfaces that provide the longitudinal and lateral control authority. Although certain other unconventional control surfaces can be explored (like drag rudders), but before them more basic control surfaces need to be sized. This sizing will be done through optimization, which is to be further built upon the work done in the previous section, where AVL provides the required aerodynamic analysis and cma-based optimization is done through optimization.

The surfaces are designed in the following order:

- The ailerons are designed first, with initial constraint of keeping the outboard end fixed as further as possible (at $y=30.6$) in the outer wing, while trying to find the smallest aileron possible.
- The remaining space available in the trailing edge along the outer wing (within structural constraints) provides the domain within which the elevator is sized. Moreover, it is made sure that the elevator and the aileron are consistent with each other.
- The rudder is sized last out of the three surfaces, as most of its demanding requirements are to be satisfied in conjunction with aileron (like for instance, steady sideslip).

The template adopted for optimizing the size of control surfaces when adopted for any of the surfaces applicable, within the structural constraints (and at respective critical flight conditions) remains similar with few alterations. There can be few other constraints based on these span divisions, like fixing one end of control surface and giving optimizer the freedom to vary the other end, to test different spans of the control surface. surfaces like the aileron are given increasingly large domain from the outboard

end till a feasible design is obtained.

The domain over which a control surface with constant chord can be laid out can be defined by the lower limit of chord fraction (here that is limited by fuel tank, obtained from Oosterom[33]) and the span in the trailing edge extends over most of the trailing edge until the hinge line is not forced to be kinked for the control surface. The whole span of domain is discretized into multiple small divisions, it is usually kept from 15 to 25 number of divisions of span, as illustrated in figure 3.4 although this figure is a schematic representation of the concept and does not include the real dimension of bounds. Each division is small enough but not too small so as to make possible design population size too large, and the optimizer can fixate on a suitable span fairly quickly into the first few iterations.

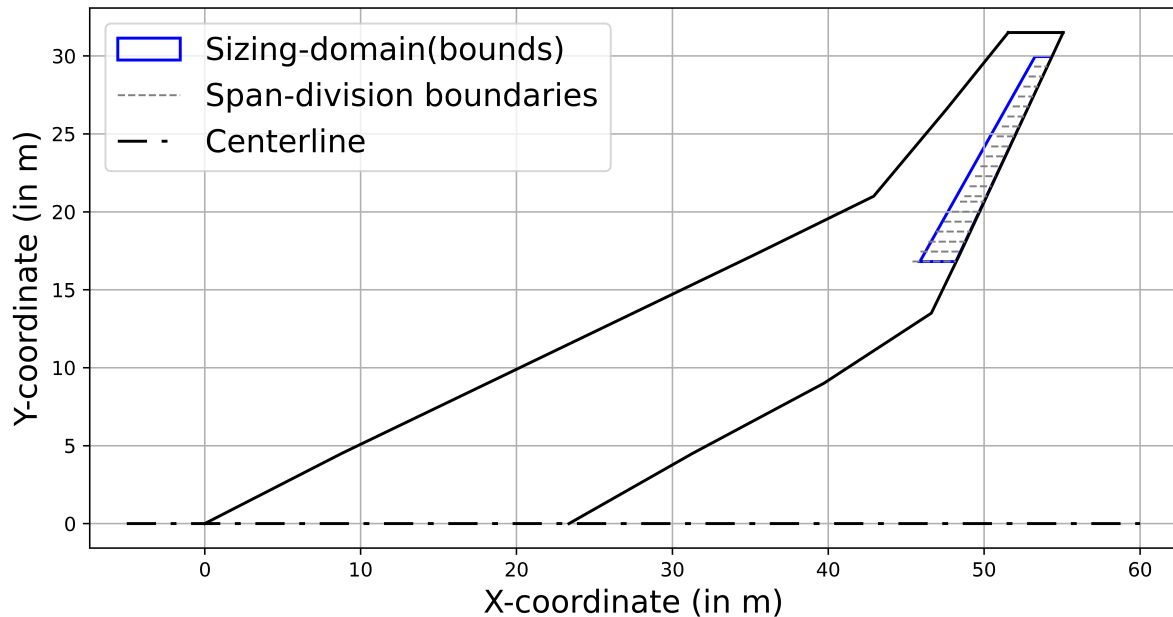


Figure 3.4: Representative domain for sizing the control surface;divisions or cells highlighted via dashes

The optimization procedure for a control surface first starts with input of initial design variables which defines the spanwise positions of inboard and outboard ends, thus the span, and the chord fraction of the hinge line. This control surface is then integrated into the geometry definition of the whole FV-1000 and the '.avl' file is constructed. The geometry is used as an input and aerodynamic analysis is done for the respective defined critical flight conditions, and all design iterations by optimizer goes through this procedure, until constraints and convergence conditions are met. The critical flight conditions are to be set for the respective control-related maneuver accordingly, with the appropriate parameters like speed, weight, and the center of gravity position, which have been discussed in Section 3.2. To elaborate on this procedure, a visual flow chart of process is illustrated in figure 3.5.

However, not all surfaces in this study will be designed using an optimization procedure such as the one explained in the flowchart above. The rudder designs in some previous handling quality related studies like those by Cappuyns[10], Joosten[26] have concluded that the rudder comes short by a fair margin, like for the OEI trim condition in Cappuyns' study and steady sideslip condition in Joosten's study, so rudders extending the full span possible over the length of the winglet should be adopted and its analysis needs to be done to verify their ability to satisfy the certification requirements. Instead of optimizing the size of rudder surface for any of certification requirements related to directional control,

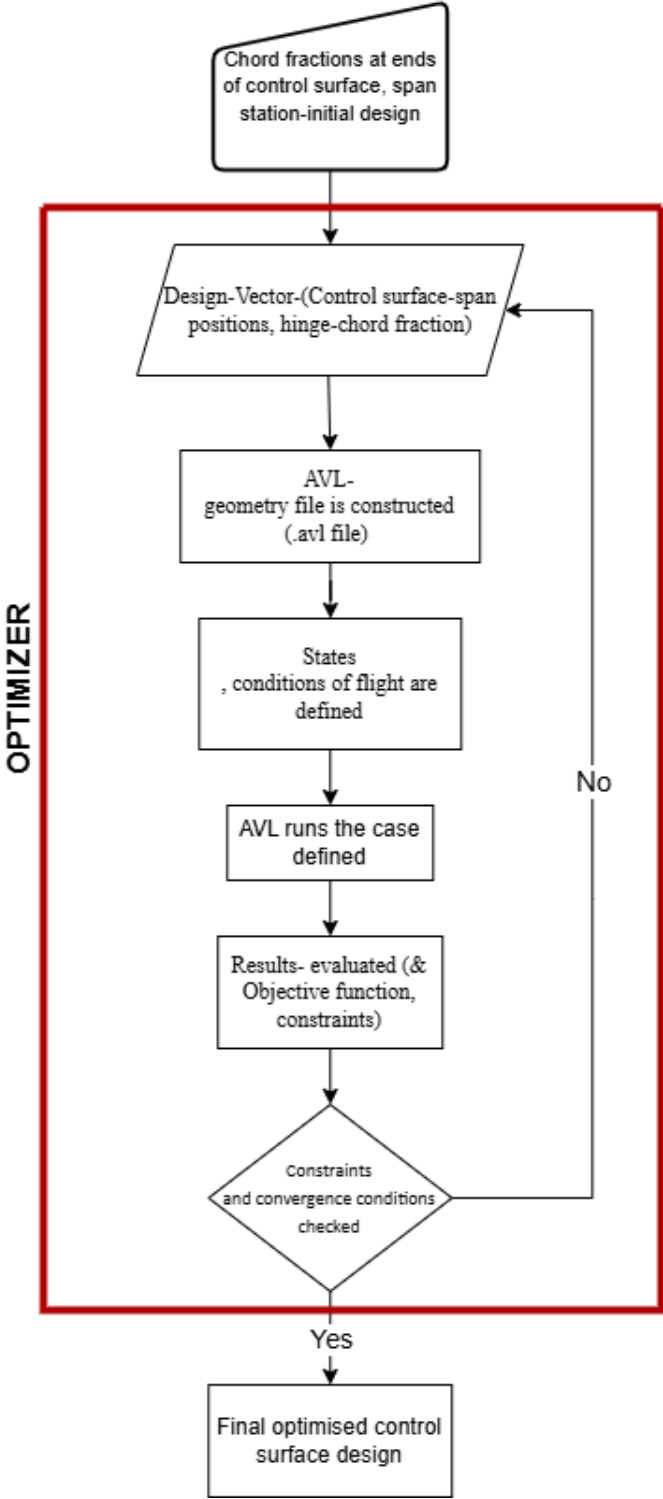


Figure 3.5: Flowchart- optimization algorithm for control surface(aileron,elevator)

first the biggest possible rudder size and few iterations of design with varying position of hinge lines can be tested to check their feasibility. Since previous studies have confirmed deficiencies in lateral control, in case the rudder is not feasible even at the largest possible size, it can cause prolonged optimization through python-based CMA optimization, and this procedure, which might take hours, might not even yield any results as feasible designs are not possible within bounds. So, this manually iterative process is opted rather than algorithm-based optimization through programming for rudder sizing.

(Note: There are certain passages throughout the thesis where original text by author is rephrased using chatgpt, used as a grammar correcting tool)

4

Validation

4.1. Stability and Control derivatives

Since there is a crucial role of stability and control coefficients in the control surface design procedure, the values predicted by AVL (Vortex Lattice Method) need to be validated against experimental data.

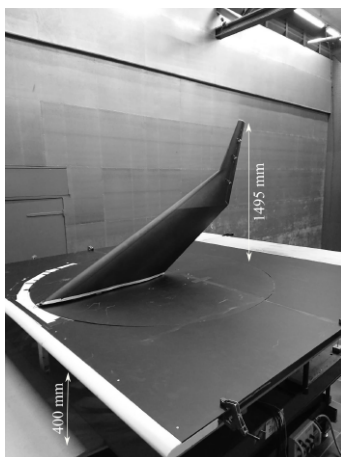


Figure 4.1: Half-Flying-V section used for wind tunnel experiment [34]

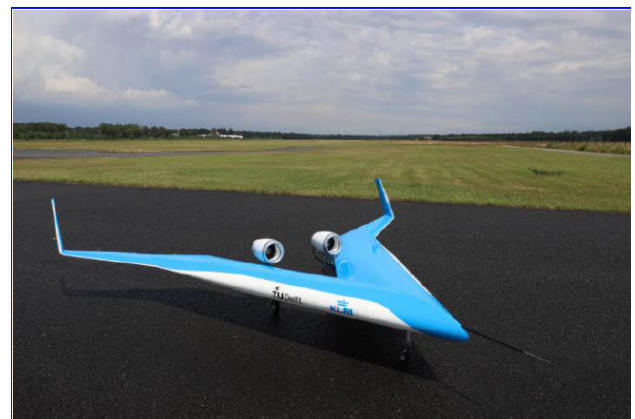


Figure 4.2: Flying V subscale model for flight test experiment [19]

The experimental data here consist of data obtained from wind tunnel tests [5] for the Flying-V half-wing model, as can be seen in Figure 4.1. The tests were conducted at a low subsonic speed of 24.4 m/s under various configurations, including a clean wing (zero control surface deflection) and combinations of elevon and rudder deflections, at a mean Reynolds number of 1.3×10^6 . Apart from this wind-tunnel experiment, there is comparison with subscale flight experiment. The flight model is 4.8% of full-scale size and its image can be seen in Figure 4.2. The flight experiment is conducted at relatively lower angle of attack ranging from 0° to 10° , sideslip or even the control surface deflection (δ_r , δ_a and δ_e), so this study can provide some dynamic coefficients of interest, but for more nonlinear effects, which occur at higher control surface deflections or angle of attack for this wind tunnel experiments are useful. The

sideslip angle is varied from $\pm 5^\circ$, elevator and aileron deflection ranges $\pm 5^\circ$ and rudder deflection is varied from $\pm 10^\circ$.

The coefficient " $C_{m_{\delta_e}}$ " (Table 4.1) at different angles is taken from the wind-tunnel experiment results by Asaro[5], including the the Experimental value of " C_{m_α} ", which is tabulated in Table 4.2. The VLM coefficients in both the tables are the results of AVL aerodynamic analysis of the same model.

Table 4.1: Comparison of Wind-tunnel and VLM results for different angles of attack of $C_{m_{\delta_e}}$

Angle of Attack [$^\circ$]	Wind-tunnel $C_{m_{\delta_e}}$	VLM $C_{m_{\delta_e}}$	Ratio: VLM/Wind-tunnel
0	-0.363	-0.617	1.698
5	-0.369	-0.614	1.664
7.5	-0.372	-0.609	1.638
10	-0.374	-0.602	1.605
15	-0.330	-0.580	1.757
20	-0.287	-0.552	1.922

Table 4.2: Comparison of C_{m_α} values: Experimental vs. VLM at $\alpha = 7.5^\circ$

	C_{m_α}
Experimental (Wind-tunnel)	-0.4788
VLM	-0.8740
Ratio: VLM / Experimental	1.8254

The above coefficients are used for comparing the longitudinal trim results between VLM and experimental (wind-tunnel) results. In Table 4.1, it can be observed with increasing AoA, there is decrease in elevator effectiveness, and the ratio of effectiveness increases with increasing AoA. Thus, it can be expected that disparity between, elevator deflections for same AoA will increase with increasing AoA. The resulting AoA and elevator deflections can be calculated by using longitudinal trim equation given below:

$$C_{m_{\delta_e}} \delta_e + C_{m_\alpha} \alpha = 0 \quad (4.0)$$

To obtain the required angles at longitudinal trim for VLM case, the case of $\alpha = 7.5^\circ$ is used as the corresponding " $C_{m_{\alpha, VLM}}$ " value for the $C_{m_{\delta_e, VLM}}$ value is only available for this value in Asaro's [5] study. The $\delta_{e, VLM}$, elevator deflection angle for VLM analysis, is calculated as follows:

$$-\frac{C_{m_{\alpha, VLM}}}{C_{m_{\delta_e, VLM}}} \times 7.5 = \delta_{e, VLM} = -10.77 \quad (4.0)$$

Similarly, the elevator deflection ($\delta_{e, exp}$) at $\alpha = 7.5^\circ$ is calculated using coefficients obtained from wind-tunnel at the same angle of attack- $C_{m_{\delta_e, exp}}$ and $C_{m_{\alpha, exp}}$. The equation 4.1 results in deflection as follows:

$$-\frac{C_{m_{\alpha, exp}}}{C_{m_{\delta_e, exp}}} \times 7.5 = \delta_{e, exp} = -9.66 \quad (4.0)$$

The ratios of VLM/Tunnel in Table 4.1, show that VLM overestimates the elevator effectiveness ($C_{m_{\delta_e}}$) compared to wind tunnel result. However, when calculating the required elevator deflection, VLM predicts a higher deflection than wind tunnel ($10.77^\circ > 9.66^\circ$), thus VLM underestimates the control authority offered by the elevator design. The required elevator deflection for trim comes more than the

experimental value by 11.55%, so it can be stated that the elevators designed based on the VLM data will be conservative designs.

Thus, the comparison of results for VLM and windtunnel by analyzing elevator and pitching moment related coefficients and computing the surface deflections(δ_e) suggest that VLM is expected to size the elevator conservatively.

Further example is investigated, to compare the VLM results and experimental values for other control authority case, which here is the steady sideslip case, to analyze the directional controllability case. The coefficients for the VLM and the experimental cases here are taken from the work of Asaro [5], where the VLM coefficients are also obtained through AVL. The coefficient derivatives involved in this case are tabulated in table 4.3, their ratio can be seen enlisted as well. To calculate the deflections of aileron and rudder required to maintain the steady sideslip at a particular sideslip angle, the equations 3.13 and 3.12 are used.

Table 4.3: Comparison of Coefficient Derivatives: Experimental vs VLM

Coefficient Derivatives	Experimental	VLM	VLM / Experimental
$C_{l\beta}$	-0.108	-0.159	1.480
$C_{n\beta}$	0.055	0.071	1.288
$C_{n\delta_r}$	0.028	0.037	1.345
$C_{l\delta_r}$	-0.008	-0.012	1.465
$C_{n\delta_a}$	-0.001	-0.011	6.760
$C_{l\delta_a}$	0.142	0.163	1.150

The plots in figure 4.3 show the variation of control deflections required for various sideslip angles. Taking the value sideslip angle (β), suppose as $\beta = 9.83^\circ$, the corresponding deflections are listed in table 4.4. The ratio obtained between Experimental and VLM values shows that the effectiveness of control surface is exaggerated, by overestimation of the control derivatives. The aileron(δ_a) and rudder(δ_r) deflections obtained for a steady sideslip case, which are obtained through the trim equations for steady sideslip, which are equations 3.13, 3.12 and 3.14. The ratio between deflections of experimental and VLM case shows opposing behaviour for aileron and rudder. The rudder deflection predicted by the VLM analysis is approximately 15% lower than that observed in the experimental case. This indicates that the control surface size estimated by VLM is undersized relative to the actual requirement. Conversely, the aileron deflection predicted by VLM exceeds the experimental value by 32%, suggesting that an aileron sized using VLM-based deflection constraints would be oversized compared to the requirement observed in experiments.

This oversizing can be quantified in terms of deflection angle. Suppose, if the aileron is designed by optimizing it at requirement-Time-to-bank, aileron deflection is limited to 25° , and the time to bank is calculated by deflecting to the maximum limit. The obtained optimized design will be functional in real/experimental case by deflecting it to $18.91^\circ (\approx 25/1.32)$. To put this in other way, for VLM analysis the limit of 25° in experimental case is equivalent to the limit of $33.04^\circ \approx 1.32 \times 25$.

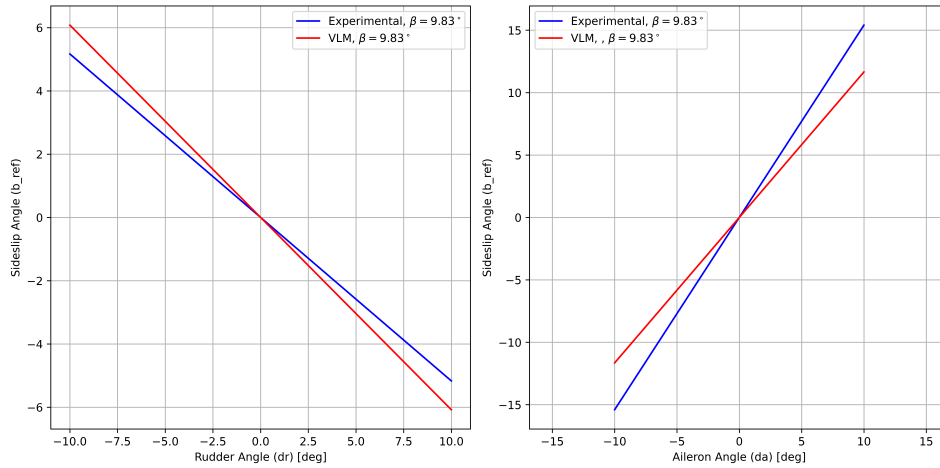


Figure 4.3: Steady-sideslip trim at a sideslip angle; Sideslip angle(β) vs. Control deflection(δ_r & δ_a) deflection comparison- Experimental & VLM-based data

Table 4.4: Deflection of rudder and aileron in subscale for $\beta = 9.83^\circ$, for steady sideslip

	Experimental Value	VLM Value	Ratio: VLM/experimental
Rudder deflection (δ_r)	-19.02°	-16.17°	0.85
Aileron deflection(δ_a)	6.38°	8.44°	1.32

4.2. Center of Gravity range determination

To assess the control authority or functioning of control surfaces it is important to have estimation of the limits and positions of center of gravity, which is done through the loading diagram or C.G (Center of gravity) envelope, which illustrates graphically the values of front and aft limit of center of gravity positions for a particular mass.

To do an estimation of the limits, the range is set with reference to the neutral point. The neutral point of an aircraft is its aerodynamic property and is independent of mass or its distribution itself. Thus for ranges of Center of gravity, taking each case and sweeping over from -8° to 15° as seen in Figure 4.4. It can be observed from the AVL's VLM analysis that few CG values show the trends in the C_m vs α plot of having the pitching moment coefficient approaching zero for all angle of attacks ranging from negative to positive.

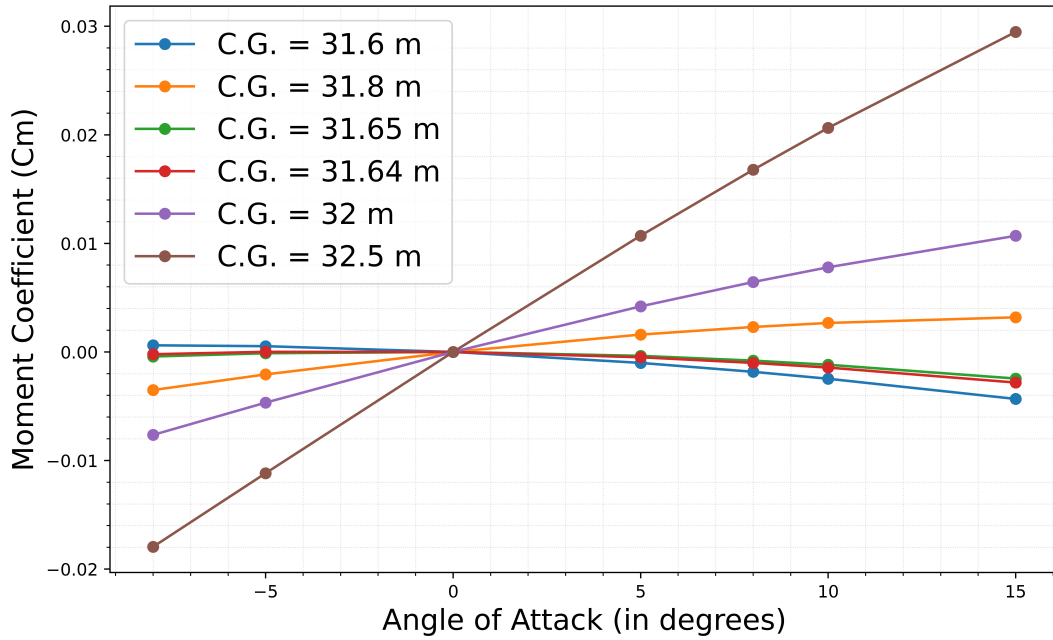


Figure 4.4: C_m vs α for various C.G. positions

For the center of gravity position $x_{cg} = 31.65\text{m}$ following are the C_m values for the stated angle of attack ranges.

$$C_m = [0.00042, 0.00012, -0.0, 0.00036, 0.0008, 0.00118, 0.00245], \text{ for } \alpha = [-8, -5, 0, 5, 8, 10, 15]$$

It is observed that for CG position at 31.65 m, the values across the negative and positive ranges are closest to zero, thus this value is chosen as neutral point.

Now that neutral point position is estimated, the C.G. position is always in front of neutral point, a safety margin is kept of 0.5 m and the width of C.G. range was estimated as about 2 m by Toorn[42], at maximum take-off weight(MTOW) the range of C.G. is estimated to be more restricted to 1 m.

Parameter	Value (in kg)
Maximum Take-off Weight (MTOW)	266000
Main Landing Weight (MLW)	$0.76 \times \text{MTOW} = 202160$
Operational Empty Weight (OEW)	127000
Payload Weight (Wp)	34000
Zero Fuel Weight (ZFW)	$\text{OEW} + \text{Wp} + 10 = 161000$

Table 4.5: FV-1000- component weight information [33]

As a full mass distribution study is not done a linear variation of forward position of center of gravity is estimated as seen in Figure 4.5. The distribution is used for finding the range of center of gravity for different mass values of aircraft, and main points of interest for the ranges are Maximum landing weight (MLW) and Maximum Take-Off Weight (MTOW), which are weights of interest to test control authority for control requirements.

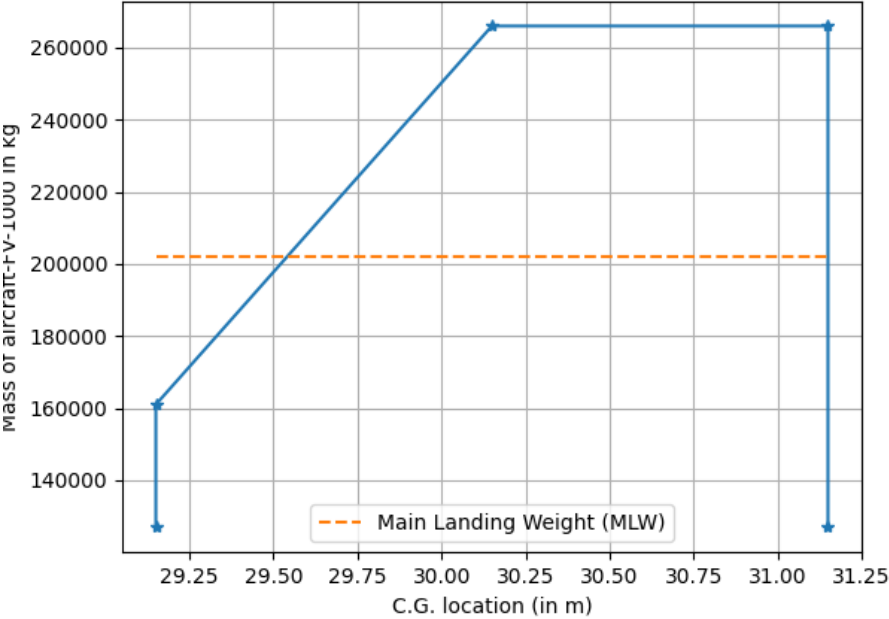


Figure 4.5: Loading diagram or C.G. Envelope

5

Results

This chapter includes the results obtained by using the methods discussed in the methodology section. First section is the aileron sizing section, where an initial aileron size is obtained by choosing a value for α_{trim} , at which optimization is done. After the span of aileron required is calculated, it over the remaining span, the elevator sizing is done. Based on this optimized elevator design, the corresponding α_{trim} is used to find updated aileron size through optimization. Third section deals with rudder sizing, the control surfaces already designed are required for simulating the certification requirements for rudder aerodynamically. Different rudder designs are aerodynamically analyzed and results are discussed accordingly. At the end of each section, expected performance of each control surface for full scale flight case is discussed based on points made in "Validation" section.

5.1. Aileron-sizing

The aileron will be sized based on a suitably selected certification requirement. In this study, the Time to Bank requirement, previously described in Section 3.2.2, is used for sizing. To evaluate this requirement using aerodynamic analysis (AVL), a corresponding trim angle of attack (α_{trim}) must be specified. Therefore, an appropriate value of α_{trim} is selected for the analysis.

5.1.1. Selection of α_{trim}

Aileron will be sized by keeping outboard end of aileron fixed at $y=30.6$ m. It is the aileron that will be first designed and then elevator in the remaining area. Since there is no way to size an initial elevator at this stage without an accompanying aileron, an approximate, reasonable value of α_{trim} is taken. This value is taken from the results of initial optimization trials tabulated in Table 3.2. The elevator design is chosen from the case: "Constant chord fraction at both ends", where optimization is done based on C_{HM} , where $\alpha_{trim} = 17.98^\circ$

5.1.2. Sizing at the selected α_{trim}

The main idea of sizing the aileron is to keep the outboard end fixed and vary the inboard end of aileron, thus the span and the hinge line position. The domain of sizing for aileron is chosen as the entire trailing edge of outer-wing from span wise position of $y=21.0$ m to $y=30.6$ m. The lower limit of hinge line chord percentage is 73.13%. The whole span is discretized into 15 divisions, and it is along these spanwise stations the ends of aileron are varied, these divisions can be seen as dashes in the figure below.

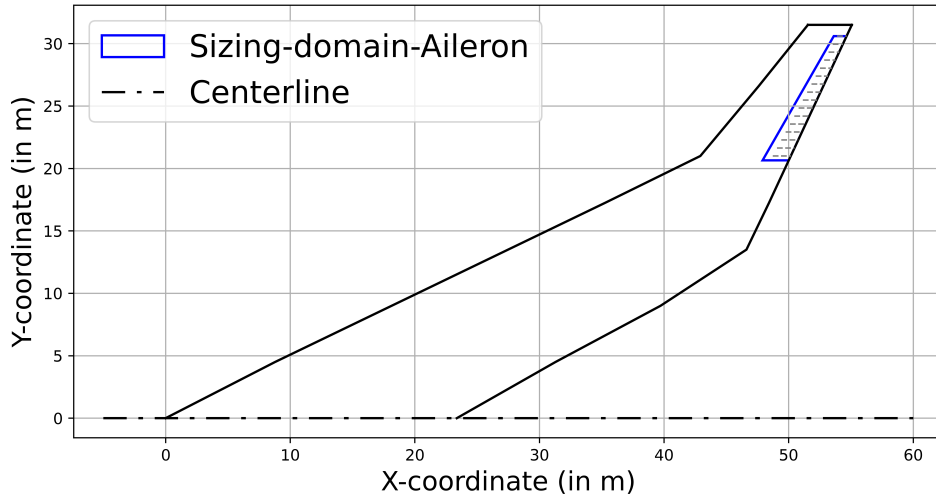


Figure 5.1: Domain for sizing the aileron;divisions or cells highlighted via dashes

A point to be noted is that small size aileron for example those spanning only 2-3 divisions will not possess enough control authority to satisfy the time to bank requirement. Therefore, it is practical to eliminate certain aileron spans early on as infeasible design options. To achieve this, the hingeline is fixed at the most forward position possible (73.13%-chord percentage). This helps reduce the design space and sampling population for the optimizer in later stages. The aileron spans in increasing order were tested for Time to bank requirement, with $\delta_a = 25^\circ$, at critical flight condition (approach speed=70.7 m/s, MLW, aft-CG=31.15 m), results are in Table 5.1. The moment of inertia (I_{XX}) about x-axis is approximated from the value of inertia at MTOW estimated by Tooren[42] on design of Oosterom[33], by using the ratio between MLW and MTOW used by Oosterom[33].

$$I_{XX,MLW} = 0.76 \times I_{XX,MTOW} \quad (5.0)$$

The angle banked in 7 seconds is calculated from equation 3.8, where $t=7$ seconds, $\delta_a = 25^\circ$, and aerodynamic coefficients from AVL analysis are put into it. The banked angle should be at least 60° , to satisfy the requirement.

Table 5.1: Effect of Aileron Span on Bank Angle Over 7 Seconds

Aileron Span (m)	Angle Banked in 7 Seconds ($^\circ$)
27.40 to 30.6	32.75
26.76 to 30.6	39.84
26.12 to 30.6	49.42
25.48 to 30.6	56.86
24.84 to 30.6	67.03

The results in the table above clearly show that the smallest aileron span that meets the "Time to Bank" requirement is from $y = 24.84$ m to $y = 30.6$ m. All smaller spans fail to satisfy this condition and can therefore be excluded from further consideration.

The angle banked by aircraft using this smallest span aileron is 67.03 degrees. Since this angle is more than 60° , and certification requires at least 60° of banking The aileron will be sized by fixing this span and letting the hingeline vary by varying the chord percentage. Now, to find the design with least hinge moment (C_{HM}), span of aileron is kept from $y=24.84$ m to 30.6 m which is the smallest span of aileron which satisfy the requirement, and the optimizer is allowed to vary the chord position of hinge line at both ends. The spanwise stations from $y=21.0$ to $y=30.6$ are numbered as $n=1$ to 15, the decision variables are defined in accordance with the discretization done and optimization is defined as follows, :

$$\begin{aligned} \text{Design vector} = & [\text{inboard spanwise station of aileron,} \\ & \text{outboard spanwise station of aileron,} \\ & \text{chord position of hingeline of control surface}] \end{aligned} \quad (5.0)$$

$$\text{Initial design vector} = [7.3, 16.2, 0.745]$$

$$\text{Lower bound} = [7.1, 16.1, 0.7313]; \quad \text{Upper bound} = [7.4, 16.4, 0.93]$$

The numbers inboard station numbers although given as fractional numbers as input to the optimizer, a rounding-off function rounds it off to lowest near integer, and appropriate inboard and outboard ends are thus assigned. The chord percentage are entered as chord fraction, and all this information is then used to build the required '.avl' file for aerodynamic analysis required during optimization. The bounds limit the span from $y=24.84$ to 30.6 m, and chord fraction can vary from 73.13% to 93%, although 93% is not a realistic design it is just set to give optimizer a wide domain to search, without limiting it to some arbitrary value of higher chord percentage. The constraints on the optimization include the limit on angle of attack & aileron deflection angle, moreover, the angle banked through in 7 seconds should be at least 60 degrees as stated before. The constraints are summarize below.

$$\alpha < 20^\circ \quad (5.0)$$

$$\phi > 60 \quad (5.0)$$

$$\delta_a < 25 \quad (5.0)$$

To make the procedure of optimization more clear, the sequence of processes is illustrated in flowchart 3.5. The initial optimization at $\alpha_{trim} = 17.98^\circ$ results in aileron design as shown in Figure 5.2, with hingeline at 79.05% chord, constant chord fraction at both ends. The optimization was terminated as result of tolerance of decision variables ($Tol_x=0.01$) being satisfied. This design is not the final proposal for aileron, as within the remaining span available in trailing edge, the elevator will be designed. The spatial discretization of domain for elevator is discussed in next section, a newer aileron will be design to be consistent with the outcome design for elevator. "Consistent" in this context means that the newly designed elevator results in a different trim angle of attack (α_{trim}). Consequently, the aileron—designed after the elevator—must be optimized based on this updated α_{trim} to ensure consistency in the overall aerodynamic configuration.

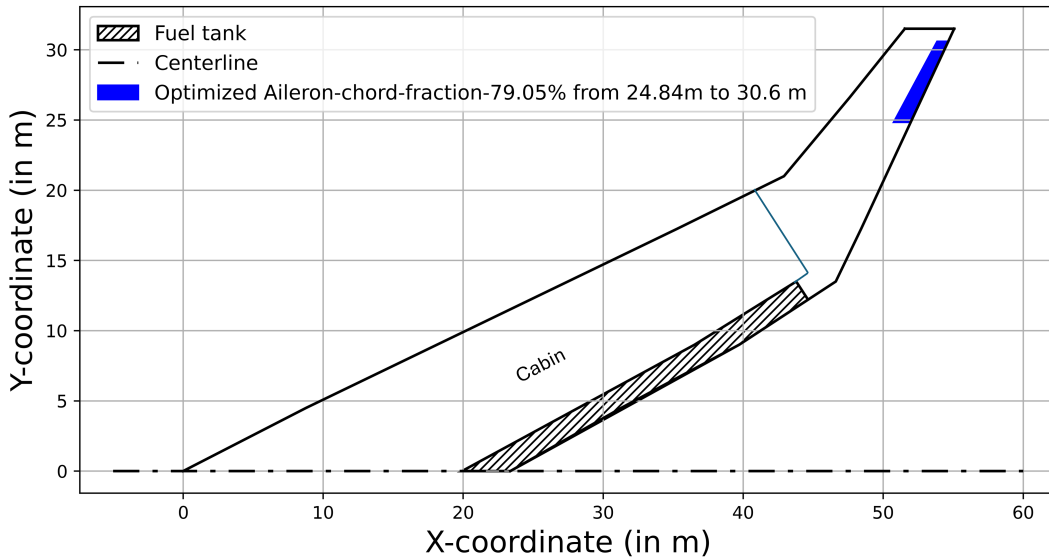


Figure 5.2: Optimized aileron, designed at $\alpha_{trim} = 17.98^\circ$

In validation section, when VLM and wind-tunnel results of aileron were compared it was observed that VLM tends to oversize the aileron, so there is a possibility of making a smaller sized aileron than the one illustrated in Figure 5.2. This aileron is optimized by keeping aileron deflection to its limit at $\delta_a = 25^\circ$, in VLM. If the comparisons made in the validation section for sub scale aircraft are applied here, and it is hypothesized that trends between VLM data and wind tunnel is equivalent to trends between full scale VLM analysis and the full scale flight behaviour, then the initial optimized aileron design can be defined differently.

Assuming that the trends observed between VLM and wind tunnel data for the sub scale aircraft also apply to the full-scale case, and that the relationship between full-scale VLM analysis and full scale flight behavior follows a similar pattern, this new aileron design can be proposed as follows in full scale conditions: "a conservative aileron design, designed via optimizing at $\alpha_{trim} = 17.98^\circ$, with aileron deflected at 18.91° ($18.91 \approx 25/1.32$, from Section 4.1), for the time-to-bank requirement". Thus, it is evident that aileron design illustrated in figure 5.2 can fulfill the time-to-bank condition requirement at $\alpha_{trim} = 17.98^\circ$, with some fraction of control authority still remaining. To quantify this remaining control authority the δ_a for both VLM and full scale flight behavior can be compared, $\delta_a = 18.91^\circ$ for full scale flight case while achieving the same requirement in VLM analysis leads to aileron deflection of $\delta_a = 25^\circ$. Thus, it can be stated that for full scale flight case, ailerons can work at 75.64% of full control authority and still execute the time-to-bank requirement maneuver.

When this optimized aileron is compared with the time to bank maneuver assessed by Cappuyns[10], the inner elevon when deflected to 10 degrees, the maneuver is done within 7 seconds (6.1 s). However, here the rudder exceed the limit deflection, as $\delta_r = 60^\circ$, as to counter side-slipping while rolling by the yaw-Stability augmentation system. In this study, the formulation of equations were taken from Kay[27], the rudder deflection required during this rolling motion is not considered. Hence it can be said that aileron in itself could prove to be enough to execute this banking maneuver, but needs a complimentary rudder which can within constraints assist in execute this banking maneuver. To estimate the performance of aileron in high angle of attack, whether the design exhibits departure tendency, LCDP- Lateral Control Departure Parameter is calculated. LCDP for this aileron, at $AoA=20^\circ$, where

$LCDP=0.1503>0$. The positive value of parameter indicates that design is spin resistant and less prone to lateral or aileron induced departure[27].

5.2. Elevator sizing

The elevator sizing is done via optimization as well, but the bounds for this control surface are set in accordance with the span of the aileron designed in the previous section. The certification requirement at which elevator is optimized is described and domain for elevator design is defined. At last the optimization procedure opted is described briefly, and results are presented with discussion. At last, the results from VLM is extrapolated to result for full-scale flight case, this discussion is supported by comparisons made in validation chapter.

The aileron, as described in the previous section, spans from $y = 24.84$ m to $y = 30.6$ m. As a result, the elevator is designed within the span limits of $y = 16.81$ m to $y = 24.84$ m. The inboard limit of $y=16.81$ m is set so as not to encroach on the fuel tank and cargo area, and even though there is kink in leading edge aircraft, the hinge line of control surface remains without any kink, a straight line. The space available for elevator sizing is illustrated in Figure 5.3. The span from $y = 16.81$ m to $y = 20.65$ m is divided into six segments, each 0.64 m long, consistent with the segment length or discretization used in the aileron sizing. The only segment not 0.64 m in length is from $y=20.65$ to $y=21$ m. In total, there are 22 segments spanning from $y = 16.81$ m to $y = 24.84$ m.

Table 5.2: Effect of Elevator Span on Trimmed Angle of Attack and Elevator Deflection

Elevator Span:(in y coordinates, metre)	Angle of Attack (°)	Elevator Deflection (°)
16.81 to 21.00	18.72	42.00
16.81 to 21.64	18.68	38.00
16.81 to 22.28	18.63	32.95
16.81 to 22.92	18.59	30.11
16.81 to 23.56	18.54	26.82
16.81 to 24.20	18.50	24.18
16.81 to 24.84	18.47	22.63

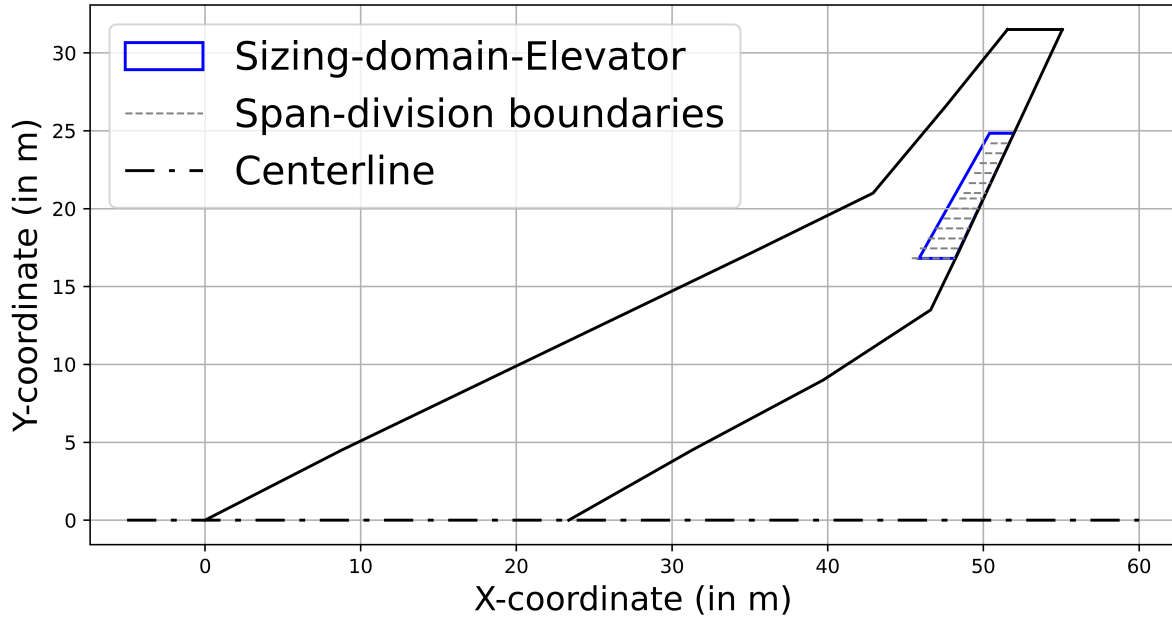


Figure 5.3: Domain for sizing the elevator; divisions or cells highlighted via dashes

The certification requirement at which elevator is sized through optimization is the longitudinal trim condition. The critical flight condition at which this longitudinal trim is simulated can be described as follows: MLW, CG is at most forward position ($x_{cg} = 29.51m$), at approach speed ($V_{app} = 70.7$). The same condition is described in Section-3.2.1. The inboard end of elevator is kept fixed at spanwise position $y=16.81$ m and span is increased in outboard direction. However, some spans of elevator are not feasible, as they will not provide enough control authority. Therefore, first spans are tested in increasing order in trim condition as tabulated in Table 5.2. The hingeline is kept at lowest chord percentage-73.13%, which means control surface is kept maximum for the given span. The following constraints are placed on elevator deflection angle (δ_e) and the angle of attack (α).

$$\delta_e < 25^\circ$$

$$\alpha < 20^\circ$$

The constraint on elevator deflection is based on limit set in Tooren's study[42] and angle of attack is limited to 20 degrees to avoid exceeding the limit where pitch break is predicted [42]. It is observed that when the elevator spans from $y=16.81$ m to $y=24.2$ m, then angle of attack at trim is 18.5 and elevator deflection angle is 24.18° , thus constraints are not violated. For elevator designs, with lesser spans than this design, the designs violate the constraints, thus are not feasible in context of longitudinal trim.

The optimization problem is defined in a way that the span varies from the inboard end (kept fixed) and the outboard end varies from $y=21.0$ m (corresponds to spanwise number=8, according to divisions in Figure-5.3) to $y=24.84$ m (limited by the adjacent smallest spanned-aileron). The bounds are set more than feasible range (from station 13 to 14) so optimizer can go through infeasible designs as well, discard them, and come up with a feasible design with minimum C_{HM} possible. The chord fraction of outboard end of elevator is part of design vector not the inboard chord fraction, it is calculated by using equation of hingeline, it can't be kept same because the presence of leading edge kink at spanwise position $y=21.0$ m. After the leading edge kink at $y=21.0$ m, chord length increases and the constant

chord fraction is not mathematically valid when control surface extends inboard of $y=21.0$ m.

$$\begin{aligned} \text{Design vector} &= [\text{outboard spanwise station of elevator,} \\ &\quad \text{chord position of hingeline of control surface at outboard end}] \\ \text{Initial design vector} &= [13.37231784, 0.853173212] \\ \text{Lower bound} &= [8, 0.731386545]; \quad \text{Upper bound} = [14.4, 0.97] \end{aligned} \quad (5.0)$$

The procedure of optimization is identical to one explained in flowchart 3.5, the constraints are on angle of attack and elevator deflection angle, these are outcomes from trimming the aircraft at the critical flight condition stated previously.

The result obtained from the optimization of the elevator done for longitudinal trim is displayed in Figure 5.4, its the red surface with hinge line at chord percentage-76.91% on the outboard end which is at outer wing. this optimized elevator spans from $y=16.81$ m to 24.84 m. This result thus introduces the spanwise position where trailing edge control surfaces over outer wing is split ($y=24.84$ m). The aircraft is trimmed at $\alpha_{trim} = 18.44^\circ$ and the elevator deflects by 23.87° . The aileron is again optimized at this new α_{trim} and a newer design is obtained. This design spans between the same spanwise positions as before ($y=24.84$ m to 30.6 m), the hingeline for this is at 78.87% chord percentage at both ends. Since the current trim angle of attack, α_{trim} , is higher than that used in the previous design optimization, the resulting aileron surface is slightly larger (78.87% compared to 79.05%). However, the increase is minimal, as the optimizer simultaneously aims to minimize the hinge moment coefficient, C_{HM} , while providing sufficient control authority to meet the time-to-bank requirement.

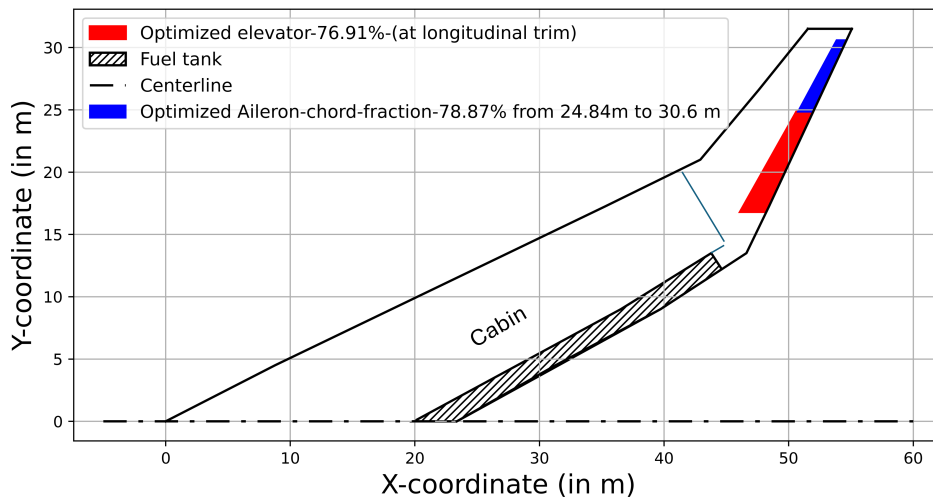


Figure 5.4: Elevator and aileron design- optimized combination

This elevator design is then checked for the longitudinal maneuver condition, for pulling up at 1.3 g. The limiting or critical flight condition for this is at approach speed, CG positioned at forward position, aircraft weighing MLW, pull-up starts from longitudinal trim position. The elevator deflects at $\delta_e = 35.47^\circ$ and $\alpha = 24.49^\circ$. These angles are calculated using two equations 3.21 and 3.22. One possible solution to keep the angle of attack within constraints ($\alpha < 20$), and check if current elevator design is feasible, is to calculate the amount of extra lift (ΔC_L) is required at the α_{trim} for this elevator design, such that the change in angle of attack ($\Delta\alpha$) and elevator deflection ($\Delta\delta_e$) does not cause these angles to exceed

the constraints. The solution of equations taking into account this additional lift estimates at least $\Delta C_{L,add} = 0.163$, required at which angle of attack goes below the 20° , but in this case is still deflected by $\delta_e = 29.04^\circ$ to execute the longitudinal pull up.

To keep the deflection of the elevator under constraint, even more additional lift will be required, this means finding the additional lift required to keep the deflection of the elevator to a maximum of 25° . This additional lift turns out to be $\Delta C_{L,add} = 0.265$, at which the angle of attack is 17.18° , and elevator deflection is 25° ($\delta_e = 24.99^\circ \approx 25^\circ$). Therefore, additional lift at trim required to execute pull up of 1.3 g and keep α , δ_e under the set constraints, is $\Delta C_{L,add} = 0.265$ instead of 0.163. This amount of additional lift ensures that the optimized design proposed in Figure 5.4, can meet the certification requirement of the longitudinal maneuver, the 1.3 g pull-up, without violating the constraints.

The design shown in Figure 5.4, if required, can be simplified further, if structurally it is easier. This simplification can be done by letting the aileron and elevator have a hinge line at the same chord percentage (76.91%), thus for the outboard end of the elevator and both ends of aileron the chord percentage becomes the same. This version of design can be seen in Figure 5.5, if closely observed and compared by Figure 5.4 the shift in chord percentage of hinge line is noticeable, it seems one single hinge line in the new version. If this newer aileron is checked for Time-to-bank condition, with aileron deflection at maximum ($\delta_a = 25^\circ$), in 7 seconds aircraft banks through 62.4° instead of 60.06° , which was case of the optimized aileron (hingeline-78.87%). Thus, with increasing aileron area, comes increase in control authority as expected.

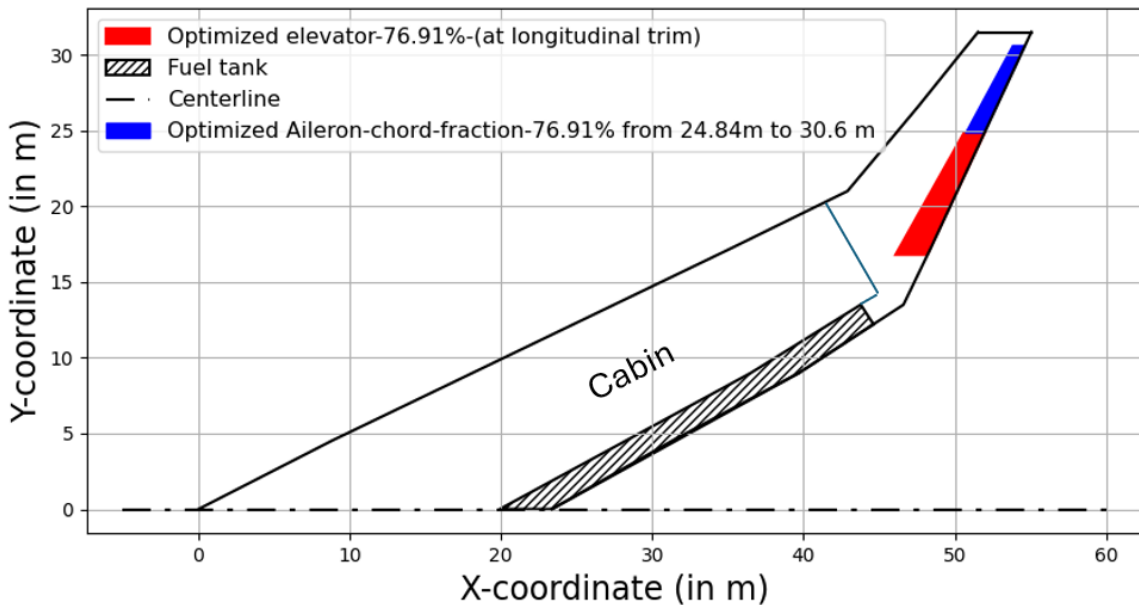


Figure 5.5: Elevator and aileron design- optimized combination, aileron's hingeline matched to elevator's hingeline

To make a comparison between the performance of elevator between VLM-analysis results and full-scale expected result, the comparison between full scale flight test result and VLM analysis done in Section 4.1 can be used as a reference. The current optimized elevator design in the VLM analysis, trims at $\alpha_{trim} = 18.44^\circ$ while it deflects to $\delta_e = 23.87^\circ$. At the same trim AoA, the deflection can be approximated for full-scale flight case, by using the ratio: $C_{m\delta_e, VLM} / C_{m\delta_e, fs} = 1.115$ and longitudinal trim equation 4.1. The deflection of the same optimized elevator design for full scale flight case comes

out to be $\sim 21.41^\circ$, thus within the constraints imposed on δ_e . To predict the deflection for full-scale case for longitudinal pull up, it comes out to be $\delta_e = 31.81^\circ$, still above the prescribed constraint of 25° . One other constraining certification requirement which is to be considered is the Take-off rotation speed. The optimized elevator is deflected to the maximum deflection chosen in this study ($\delta_e < 25^\circ$), and $AoA = -3.92$ is a result of nose and main landing gear length, as discussed previously in 3.2.6. The rotation speed for most forward CG position ($x_{cg} = 30.15$), MTOW comes out to be 38.15 m/s. This value is about 50% of the maximum constraint value set on it ($(V_{2MIN} - 5) \sim 76.6 \text{ m/s}$). The take-off rotation speed coming this low in comparison to the limit can be explained if it is put in context of the result for the same in Tooren's study[42]. In that study for the optimized FV-1000 design, the take-off rotation speed keeps on decreasing with rearwards shift in CG, and to a higher extent. This higher decrease in rotation speed can be explained by the fact that the elevon employed as elevator in this case spans almost entire outer wing in contrast to the optimized elevator in this study which extends $\sim 58\%$ of outer wing span.

When comparing the optimized elevator design to the elevon configurations from Cappuyns [10] for longitudinal control requirements, the trim deflection angles were found to be significantly lower in the latter: $\delta_{e,1} = 13^\circ$ for elevon-1 alone, and $\delta_{e,1} = 7.8^\circ$ when both elevons were used, compared to a deflection of 23.87° required by the optimized elevator. This difference may be attributed to several factors: the control surfaces in Cappuyns' design had a larger chord (with the hingeline at 68% chord instead of 73%), a higher approach speed was assumed (78 m/s compared to 70.7 m/s in this study), and the elevator span was also larger. Even the span of elevon-1 (inner elevon) (from $y = 12.88 \text{ m}$ to $y = 23.31 \text{ m}$) exceeds that of the optimized elevator (from $y = 16.81 \text{ m}$ to $y = 24.84 \text{ m}$). Both these larger sized elevons of Cappuyns with deflection of 14° are able to pull-up 1.39 g. However, the optimized elevator even when accompanied by deflection of optimized aileron does not satisfy 1.3 g pull-up requirements as CG chosen in this case is a bit more forward than Cappuyns and approach speed is noticeably lower.

This justifies the integration of a high-lift device operating in conjunction with the elevator. The need for these devices arise so the angle of attack can be reduced, and at lower angles of attack, control authority of aileron increases. Another method of decreasing this AoA is to increase the approach speed (current value assumed in this study- $V_{app} = 70.7 \text{ m/s}$), which reduces the required α_{trim} , thus satisfying all the constraints..

5.3. Rudder sizing

The rudder for an aircraft cannot be sized by itself as a separate task, it needs the accompanying aileron and elevator design. This is attributed to the fact that so much of rudder usage in control-based maneuvers is done simultaneously with the other two control surface. Since, in previous two sections aileron and elevators are designed with their respective optimization procedures, the designs from those two sections, particularly aileron, are tested with possible rudder designs to check their viability in satisfying the relevant certification requirements. Rudder designs as discussed in previous studies have been found lacking in terms of control authority for particular control requirements, for instance Cappuyns[10] for OEI trim and Joosten[26] for his rudder design concluded noncompliance for both OEI condition and steady sideslip.

The sizing of the rudder for the Flying-V as discussed in section 3.4, will not involve optimizing the span and chord for the control surface, but chosen iterations of the rudder designs will be tested for the

relevant certification requirements. In a study consisting of optimizing the winglets by Amur[3], chord fraction of the rudder is maximum 30%, constrained due to the aft spar, which was also the case in the study by Faggiano[18]. Both of these studies place the aft spar at chord fraction of 0.7 ($x/c=0.7$).

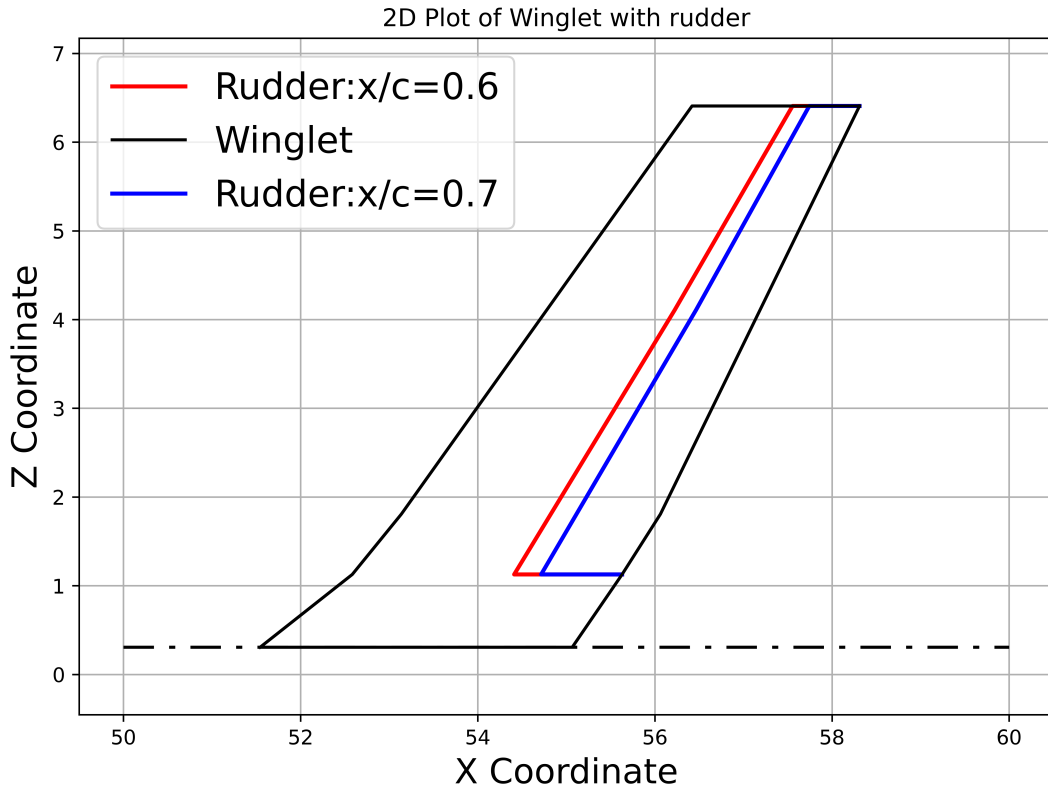


Figure 5.6: Two-dimensional side-view of Rudder designs with hinge line at chord fraction-0.6(red) & 0.7(blue)

$$C_Y = 0 = \frac{W}{qS} \cos(\gamma) \phi + C_{Y\delta_r} \delta_r + C_{Y\delta_a} \delta_a \quad (5.0)$$

$$C_{l\delta_r} \delta_r + C_{l\delta_a} \delta_a = 0 = C_l \quad (5.0)$$

$$C_{n\delta_r} \delta_r + C_{n\delta_a} \delta_a + C_{nOEI} = 0 = C_n \quad (5.0)$$

First, various rudder designs are checked if they are able to trim the aircraft in OEI condition. The angles of interest in this case are δ_e , δ_a & ϕ . These angles are calculated using equations for side force, rolling moment and yawing moment. The three equations used for calculating the three unknowns: controls surface deflections (δ_a , δ_r) and the bank angle (ϕ) are equations 5.3, 5.3 and 5.3. The thrust of one engine which is operating, used to calculate " C_{nOEI} ", is taken from the work of Asaro et al.[6], thrust taken is for MTOW, obtained from a thrust to weight ratio graph. All variations of the hinge line chord fractions from 0.6 to 0.9 in increments of 0.05, for both the forward and aft positions of CG at the minimum control speed- V_{mc} weighing at MTOW are tested. The critical flight condition in work of Tooren[42] specified the speed as V_{mc} and weight as MTOW. The minimum control speed is estimated as 1.13 times the stall speed[2], stall speed is based on maximum lift coefficient, which is taken as 1.1[9]. The value of V_{mc} is calculated to be 74.21 m/s. The rudder designs for each iteration span over the whole winglet as shown in 2-D side view of winglet planform as show for two chord fractions (0.6,0.7) in the Figure 5.6. The OEI trim condition control deflection results are presented in Figures 5.7a (for rudder deflection)

and 5.7b (for aileron angles) for forward CG and aft CG-OEI trim condition respectively.

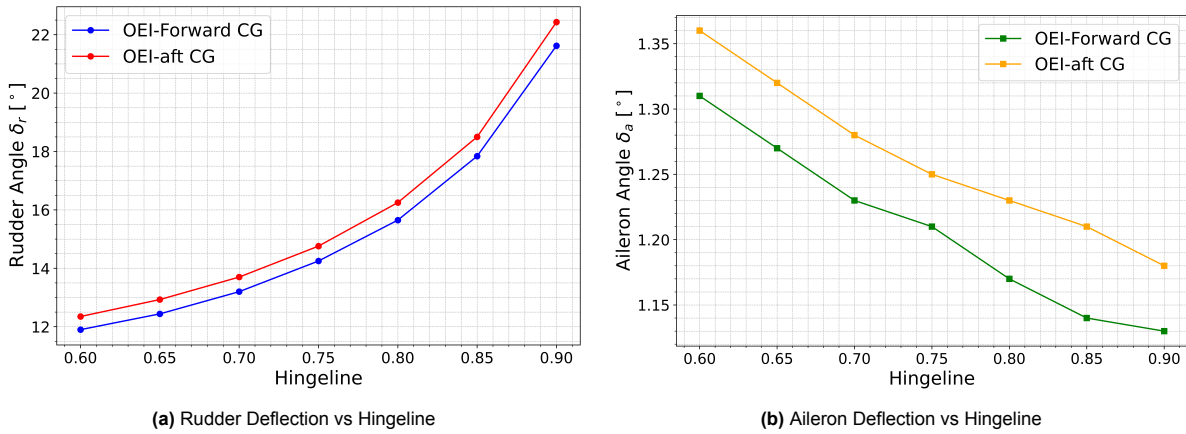


Figure 5.7: Comparison of deflections (absolute values) for OEI trim condition at forward CG ($x_{cg} = 30.15$ m) & aft CG ($x_{cg} = 31.15$ m)

From the results in the figures above for OEI, it can be observed that the critical condition is when CG is placed at the aft position, with deflections of both aileron and rudder being more for this case than for forward CG. The rudder deflection for hinge line-0.7 for aft CG case is -13.7° , larger than the forward CG case (-13.2°). Thus, it is OEI-trim at aft CG, which requires more control authority. OEI trim has been shown to be plausible for a variety of rudder sizes. All chosen rudder iterations (hinge line from 0.6 to 0.9), which are analyzed at the OEI trim conditions, do not need to be deflected above the imposed limit of 30° on rudder deflection angle(δ_r).

$$\beta = \tan^{-1} \left(\frac{Cw_{vel}}{V_{mc}} \right) \approx 9.83^\circ \quad (5.0)$$

The other requirement which must be fulfilled is the steady side-slip. Similar to the OEI trim condition, for steady sideslip deflections are evaluated for variation of rudder sizes at forward and aft CG positions, speed at V_{mc} , weight MTOW. The sideslip angle is calculated according to V_{mc} , and the cross-wind component(Cw_{vel}) is decided based on values specified in regulations CS-25, 28th amendment[2], which finally yields the sideslip angle to be $\beta = 9.83^\circ$, as can be observed from Equation 5.3. The data for both CG positions is plotted in Figures 5.8a for rudder deflection and 5.8b for aileron deflection.

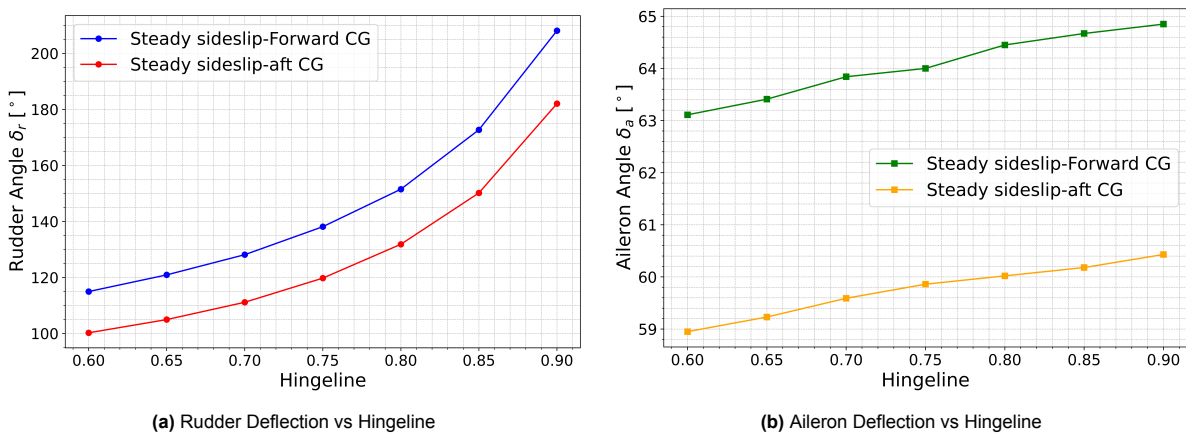


Figure 5.8: Deflections(absolute values) for steady sideslip condition at aft CG ($x_{cg} = 31.15$ m) & aft CG ($x_{cg} = 31.15$ m)

From the results of the control surface deflections plotted in the figures above, it is quite clear that none of the rudder designs can satisfy the constraints on aileron ($\delta_a < 25^\circ$) and rudder deflections ($\delta_r < 30^\circ$). It seems from results that deflections, both the rudder (δ_r) and aileron (δ_a) are more for forward CG in the Steady sideslip case, so this CG position is more demanding and thus the critical flight condition for the Steady sideslip requirement. Since for forward CG position, while trimming the aircraft with the elevator design (optimized one), $\alpha_{trim} = 21.42^\circ$, the deflections of the control surfaces are calculated for lower AoA values. This is done with the objective of finding out whether the deflections violate the constraints. The results for the design of the rudder with chord fraction 30% are shown in Table 5.3. This particular position of hinge line is chosen as previous studies have stated that the position of the aft spar is at 70%.

Table 5.3: Deflection angle at various AoAs for chord fraction=0.7, at forward CG ($x_{cg} = 30.15$), V_{mc} , mass-MTOW

AoA [°]	Beta [°]	Aileron Angle [°]	Rudder Angle [°]
0.0	9.83	-1.84	-17.46
1.0	9.83	-5.06	-16.60
2.0	9.83	-8.25	-16.18
3.0	9.83	-11.40	-16.19
4.0	9.83	-14.52	-16.60
5.0	9.83	-17.61	-17.55
6.0	9.83	-20.67	-18.99
7.0	9.83	-23.71	-20.78
8.0	9.83	-26.73	-23.23
9.0	9.83	-29.66	-26.32
10.0	9.83	-32.63	-29.81
11.0	9.83	-35.53	-34.01

The results show that it is when the angle of attack is $\alpha = 7^\circ$, the aileron ($\delta_a = 23.71^\circ < 25^\circ$) and rudder deflections ($\delta_r = 20.78^\circ < 30^\circ$) are under the limiting value. It seems from the results of Table 5.3 that an increase in the angle of attack depletes the rudder effectiveness. In fact, a previous study done on winglet and rudder deflection by Johnson[24] concluded that change in AoA, reduced the magnitude of rudder control derivatives ($C_{Y_{\delta_r}}$, $C_{n_{\delta_r}}$ and $C_{l_{\delta_r}}$) significantly. Moreover, changes in airspeed also reduced the magnitude of those derivatives, but even the maximum change caused is lesser than the change caused by AoA changing from 0° to 20° . So, to decrease the α_{trim} , one approach can be to increase the value of V_{mc} , which in turn means increasing the stalling speed or the approach speed as well. These changes can help to tackle the steady sideslip condition while keeping control surface deflections under constraints. Any design change apart from changing the chord fraction of the hinge line in the rudder (0.7 considered as the lower limit in previous studies[18][3]) is only further possible when the winglet design is modified, which is beyond the scope of this study as control surfaces are to be sized within limits of structural constraints such as the aft spar being the limiting factor in this case.

If the relation between rudder deflection angle (δ_r) for VLM analysis and wind-tunnel results are hypothesized to be similar to ratio of deflections for the VLM full scale model analysis to the full scale flight case, certain approximations can be made for the performance of a rudder design analyzed in AVL. In 'Validation' section, it was discussed that VLM predicts a rudder deflection angle for a geometry, which is 15% less than the deflection predicted by using aerodynamic coefficients obtained from wind-tunnel results. Considering the hypothesis made, this means that the deflection of a rudder with hinge line at 70% chord percentage (lower limit), $\delta_r = 13.7^\circ$ (absolute value) at OEI trim condition will be equiva-

lent to $\delta_r = 13.7 \times (1/0.85) = 16.11^\circ$ for full scale flight. Thus, rudder design with hinge line at 70% chord percentage possesses enough control authority to comply with the OEI requirement, while the $\delta_r = 16.11 < 30^\circ$. However, for the steady sideslip requirement, the rudder sized (even the maximum rudder size, $x/c=70\%$) misses compliance by a significant margin. As discussed before, the rudder is undersized for full-scale flight case, the rudder design will not comply with steady sideslip requirement by even bigger margin than predicted through VLM analysis.

The optimized design when compared against the result of optimization done by Tooren[42]. the control surface layout opted by Tooren is illustrated in Figure 2.4, are shown to be non-compliant to both the requirements- Steady sideslip & OEI trim but Tooren's design satisfies both requirements. Tooren's rudder design consists of 40% chord of winglet, spans full length, while in this study hingeline is placed at 70% chord, so this design is smaller in terms of the rudder's chord. Moreover, in Tooren's optimized design, fin is notably increased in length from 7 m to 9.05 m, which provides the extra control authority required to satisfy the lateral requirements. However, in the same study it was recommended that structural feasibility was not taken into consideration. In this study the fin length is about 7.9 m, and it is only the control surface design which is varied within bounds (like the aft-spar) of design based on Laar's study[28]. Thus, this increase in winglet size can provide possible solution to deficiency in steady sideslip case.

Although not directly related to control authority or power the value of parameter-' $C_{n_{\beta_{DYN}}}$ ' indicates the static directional stability, and also the yaw departure tendency. For current configuration this value is positive ($0.335 > 0$) thus this design is expected to display minimal yaw departure at high angles of attack. When both the LCDP value ($LCDP = 0.1503$) and $C_{n_{\beta_{DYN}}}$ are considered together, according to Weissman chart these values together fall in zone-A of Weissman chart, thus this aircraft configuration of FV-1000 is in "non-departure zone"[8].

6

Conclusion and Recommendations

6.1. Conclusion

The objective of this study was to find the optimal or suitable sizing of control surface for the Flying-V aircraft to be specific FV-1000. To achieve the objective first the relevant certification requirements put forth by agencies such as EASA(CS-25,28th Amendment) were gathered and their mathematical equations were presented. For the aerodynamic analysis required in the control surface sizing process, AVL was chosen as the primary tool. Since most control authority assessments are conducted at low speeds—such as approach speed (V_{app}) and minimum control speed (V_{mc})—AVL is considered sufficiently accurate and appropriate for this purpose.

A comparison between drag coefficient (C_D) and hinge moment coefficient (C_{HM}) as potential objective functions for elevator optimization revealed that C_{HM} provides a more effective option. Moreover, constant chord fraction is used to define every control surface in this study, which also ensures straight spars instead of spar with kinks. The objective function for optimizing the hinge moment coefficient (C_{HM}) was used to size the aileron and elevator. These control surfaces were then individually optimized to meet their specific design requirements. The outer wing, ranging from $y = 21, \text{ m}$ to $y = 30, \text{ m}$, was divided into 15 segments for optimization. First, in case of aileron, an initial optimized design is obtained extending from $y=24.84 \text{ m}$ to $y=30.6 \text{ m}$, the smallest feasible span, with the hinge line at 79.05%(at $\alpha_{trim} = 17.98^\circ$).The optimization was done by fixing the span and letting the hinge line position vary.The certification requirement chosen for the aileron optimization is the time-to-bank maneuver. When comparison of this VLM-based design is done to its full-scale flight performance, it is predicted that this design will be able to satisfy the Time-to-bank requirement with approximately 75% of total control authority in full-flight case.

After the initial sizing of aileron, elevator was designed using the remaining available control surface space as its domain.The remaining space is also discretized spanwise, each division measuring 0.64 m same length as done for aileron. The optimized elevator spans from $y=16.81$ to $y=24.84 \text{ m}$, with constant chord percentage at 76.91%. While this elevator configuration achieved longitudinal trim, it failed to comply with the longitudinal maneuver-pull up requirement, due to AoA exceeding limit of 20° . This

highlights the need for an additional lift-generating device, which can through additional lift, keep both AoA and δ_e below the constraint limits ($\delta_e < 25^\circ$ & $\alpha < 20^\circ$). However, based on validation discussion for elevator, the optimized elevator is predicted to be deflected by magnitude of 21.41° for longitudinal trim, even for pull-up this deflection comes out to be $-\delta_e = 31.81^\circ$, still violating the constraint. Thus, it is a requirement to decrease the AoA, which can help decreasing the required ' δ_e '.

The rudder design was previously found to be limiting for certain conditions in some previous studies as mentioned in previous sections. As a result, a manual, iterative approach was adopted to analyze various selected rudder configurations. The rudder, when combined with the proposed aileron, is sufficient to meet the One Engine Inoperative (OEI) trim requirement. However, it fails to meet the steady sideslip condition by a significant margin. This is the case for rudder with hinge line at 70% chord percentage, thus biggest sized rudder, based on constraint imposed by aft spar. When the rudder deflection obtained from VLM are extrapolated to full scale flight case, in case of OEI trim the rudder deflection remain within the limit of 30° . However, for Steady-sideslip, the full scale rudder deflection is even more, thus compliance for this requirement is missed by bigger margin.

A notable trend observed is the sharp decline in rudder's control authority with increasing angle of attack (AoA), similar to decrease in rudder effectiveness with AoA predicted in study by Johnson[24]. This further emphasizes the need to reduce AoA during critical conditions, reinforcing the requirement for a high-lift device. An alternative solution could be the incorporation of drag-based control devices, such as split flaps or split ailerons (ruddervons), which could enhance directional control authority while serving the roles of both aileron and rudder. To summarize, aileron design proposed in this thesis is expected to be function for the full scale flight as well, while the elevator and rudder design, need some structural change(change of winglet design) or assist from other control device to function within the constraints.

6.2. Recommendations:

The results of this study, do give some control surface design which should satisfy the certification requirements like aileron, at the same time control surfaces like elevator and rudder fail to comply with some certification requirements, without structural or design changes, or adding other control surfaces for assistance. However, there are results in this study upon which further research can be built,

- Future studies should include the influence of the landing gear on aircraft stability derivatives. This was not accounted for in the current AVL vortex lattice model due to its limitations and would require RANS simulations or experimental data for more accurately capturing this effect.
- A re-evaluation of OEI conditions is necessary if there is any change in the engine's spanwise position in future design iterations, as this would affect control requirements.
- The identified need to reduce AoA for effective rudder performance, along with the elevator's inability to support the pull up maneuvering, justifies the need for a dedicated high-lift device study. This device should be designed to work in conjunction with the current control surface configuration—or an improved version of it—to confirm it can assist the control surfaces in fulfilling certification requirements.
- One potential improvement could be the integration of a split flap into the existing aileron-elevator

combination. This can be achieved by splitting the outboard control surface, which here is the aileron and installing a split flap in the outer section of the proposed aileron. High-fidelity simulations should be used to assess the effectiveness of this configuration, to produce results of higher accuracy than VLM analysis.

- This study primarily focused on the sizing of control surfaces. However, these single continuous surfaces—originally sized as ailerons and elevators—can be divided into multiple segments. Subsequently, a control allocation study can be performed for these segmented control surfaces, with control mixer where they can serve as both aileron and elevator (elevon).
- The exploration of increasing stability by using a Stability Augmentation System (SAS) with set of feasible control surfaces can be pursued in future. This can help in fulfilling any insufficiency in inherent stability characteristics of the aircraft and even increase control authority as illustrated to an extent by Joosten [26], where required control deflections can be decreased for fulfilling the requirements.

References

- [1] ACARE - Advisory Council for Aviation Research and Innovation in Europe. *Time for Change: FlightPath 2050*. https://www.acare4europe.org/wp-content/uploads/2024/04/Time_for_change_FlightPath_2050-7.pdf. 2024.
- [2] European Union Aviation Safety Agency. *Certification specifications and acceptable means of compliance for large aircraft (CS-25)*. Vol. Amendment-28. 2023.
- [3] Arjav Anand Amur. "Multi-objective Aerodynamic Assessment and Optimization of Winglets for the Flying-V Aircraft Configuration". MSc Thesis. Delft University of Technology, May 2023.
- [4] John D. Anderson. *Fundamentals of Aerodynamics*. 5th. McGraw-Hill Education, 2006.
- [5] S. Asaro and R. Vos. "Synthesis of the Aerodynamic Model of a Flying Wing Aircraft". In: *AIAA Science and Technology Forum and Exposition, AIAA SciTech Forum 2025*. Article AIAA 2025-0852. American Institute of Aeronautics and Astronautics Inc. (AIAA), 2025. DOI: 10.2514/6.2025-0852.
- [6] Salvatore Asaro et al. "Control Surface Allocation Based on Offline Handling Quality Simulations for a Flying Wing Aircraft". In: *AIAA Science and Technology Forum and Exposition, AIAA SciTech Forum 2025*. Article AIAA 2025-2475. American Institute of Aeronautics and Astronautics Inc. (AIAA), 2025. DOI: 10.2514/6.2025-2475.
- [7] J. Benad. "The Flying V - A new Aircraft Configuration for Commercial Passenger Transport". In: *Deutscher Luft- und Raumfahrtkongress 2015*. Rostock, Germany, 2015, pp. 1–8. DOI: 10.25967/370094. URL: <https://doi.org/10.25967/370094>.
- [8] Lucky Bose, Isfaq Ahmed Rafsun, and Junquan Fu. "Research on stability for blended-wing-body aircraft". In: *World Journal of Advanced Research and Reviews* 23 (Oct. 2024), pp. 2919–2932. DOI: 10.30574/wjarr.2024.23.3.2961.
- [9] G. Bourget. "The effect of landing gear implementation on Flying V aerodynamics, stability and controllability". Thesis. Delft University of Technology, 2020.
- [10] T. Cappuyns. "Handling Qualities of a Flying V Configuration". Thesis. Delft University of Technology, 2019.
- [11] J. R. Chody, J. Hodgkinson, and A. M. Skow. "Combat Aircraft Control Requirements for Agility". In: *AGARD Conference Proceedings No. 465*. Advisory Group for Aerospace Research and Development, Oct. 1989.
- [12] European Commission. *Flightpath 2050: Europe's Vision for Aviation*. European Commission, 2011. URL: <https://transport.ec.europa.eu/system/files/2016-09/flightpath2050.pdf>.
- [13] Yann Denieul. "Preliminary Design of Control Surfaces and Laws for Unconventional Aircraft Configurations". PhD thesis. Institut Supérieur de l'Aéronautique et de l'Espace (ISAE-SUPAERO), 2016. URL: https://depozit.isae.fr/theses/2016/2016_Denieul_Yann_D.pdf.

- [14] Mark Drela. *AVL User Primer*. Accessed: Feb 20, 2025. URL: https://web.mit.edu/drela/Public/web/avl/AVL_User_Primer.pdf.
- [15] Mark Drela. *Flight Vehicle Aerodynamics*. Massachusetts Institute of Technology Press, 2014.
- [16] A. E. Eiben and J. Smith. "From Evolutionary Computation to the Evolution of Things". In: *Nature* 521.7553 (May 2015), pp. 476–482.
- [17] B. Etkin. *Dynamics of Atmospheric Flight*. New York: John Wiley & Sons, Inc., 1972.
- [18] F. Faggiano. "Aerodynamic Design Optimization of a Flying V Aircraft". MA thesis. Delft University of Technology, 2016.
- [19] A. R. García et al. "Aerodynamic Model Identification of the Flying V from Sub-Scale Flight Test Data". In: *AIAA SciTech*. San Diego, United States of America, 2022. DOI: 10.2514/6.2022-0713. URL: <https://doi.org/10.2514/6.2022-0713>.
- [20] D. C. Garmendia et al. "Assessment of Electrically Actuated Redundant Control Surface Layouts for a Hybrid Wing Body Concept". In: *14th AIAA Aviation Technology, Integration, and Operations Conference, AIAA Aviation*. American Institute of Aeronautics and Astronautics, 2014.
- [21] Nikolaus Hansen, Sibylle Müller, and Petros Koumoutsakos. "Reducing the Time Complexity of the Derandomized Evolution Strategy with Covariance Matrix Adaptation (CMA-ES)". In: *Evolutionary computation* 11 (Feb. 2003), pp. 1–18. DOI: 10.1162/106365603321828970.
- [22] Hansen, Nikolaus. *CMA-ES Python Package*. <https://pypi.org/project/cma/>. Accessed: Mar. 12, 2025. 2025.
- [23] J.M.T Horwitz. "Parametric Design of the Flying-V Winglets for Improved Lateral-Directional Stability and Control". MSc Thesis. Delft University of Technology, 2021. URL: <http://resolver.tudelft.nl/uuid:d7513b36-b9fd-4f8a-8726-f5c7ee7f3a6b>.
- [24] Nelson A. Johnson. "Effect of Winglet Integration and Rudder Deflection on Flying-V Aerodynamic Characteristics". Thesis. Delft University of Technology, Jan. 2021.
- [25] D. E. Johnston and R. K. Heffley. "Investigation of High AOA Flying Quality Criteria & Design Guides". In: *AFWAL Technical Report AFWAL-TR-81-3108*. Air Force Wright Aeronautical Laboratories, Dec. 1981.
- [26] Sjoerd Joosten. "Piloted Assessment of the Lateral-Directional Handling Qualities of the Flying-V". MSc Thesis. Delft University of Technology, Apr. 2022.
- [27] Jacob Kay et al. "Control Authority Issues in Aircraft Conceptual Design: Critical Conditions, Estimation Methodology, Spreadsheet Assessment, Trim and Bibliography". In: 1996. URL: <https://api.semanticscholar.org/CorpusID:110883452>.
- [28] Yuri Alexander Laar. *Aerodynamic Design of a Flying V Aircraft in Transonic Conditions*. 2023. URL: <http://resolver.tudelft.nl/uuid:591093b2-5cdc-41c5-b564-3786f43d51db>.
- [29] Nikki van Luijk. "Constrained Aerodynamic Shape Optimisation of the Flying V Outer Wing". MSc Thesis. Delft University of Technology, Mar. 2023.
- [30] Bruno Mialon, Thierry Fol, and Cyril Bonnaud. "Aerodynamic Optimization of Subsonic Flying Wing Configurations". In: *20th AIAA Applied Aerodynamics Conference*. June 2002. DOI: 10.2514/6.2002-2931.
- [31] Tigran Mkhoian et al. "On-line Black-box Aerodynamic Performance Optimization for a Morphing Wing with Distributed Sensing and Control". In: *IEEE Transactions on Aerospace and Electronic Systems* (2023).

- [32] Ed Obert. *Aerodynamic Design of Transport Aircraft*. IOS Press, 2009.
- [33] W.J. Oosterom. *Flying-V Family Design*. 2021. URL: <https://resolver.tudelft.nl/uuid:9e8f9a41-8830-405d-8676-c46bf6b07891>.
- [34] M. Palermo and R. Vos. "Experimental Aerodynamic Analysis of a 4.6%-Scale Flying-V Subsonic Transport". In: *AIAA SciTech*. Orlando, United States of America, 2020. DOI: 10.2514/6.2022-0713. URL: <https://doi.org/10.2514/6.2022-0713>.
- [35] Marco Palermo. "The Longitudinal Static Stability and Control Characteristics of a Flying V Scaled Model: An Experimental and Numerical Investigation". To be defended publicly on February 27, 2019 at 13:00. Thesis. Delft University of Technology, 2019.
- [36] P. Pošík, W. Huyer, and L. Pál. "A Comparison of Global Search Algorithms for Continuous Black Box Optimization". In: *Evolutionary Computation 20.4* (Dec. 2012), pp. 509–541.
- [37] PyAVL-Wrapper Contributors. *PyAVL-Wrapper Python Package*. <https://pypi.org/project/pyavl-wrapper/>. Accessed: Mar. 12, 2025. 2025.
- [38] Daniel P. Raymer. *Aircraft Design: A Conceptual Approach*. American Institute of Aeronautics and Astronautics (AIAA), 1992, p. 115.
- [39] C. Roos. *Roll Architecture Optimisation Method and Tool*. Airbus Internship Report. Toulouse, France: Airbus, 2003.
- [40] Riccardo Torelli et al. "Piloted Simulator Evaluation of Low-Speed Handling Qualities of the Flying-V". In: *AIAA SCITECH 2022 Forum* (Jan. 2023). DOI: 10.2514/6.2023-0907. URL: <https://doi.org/10.2514/6.2023-0907>.
- [41] Egbert Torenbeek. *Advanced Aircraft Design: Conceptual Design, Analysis and Optimization of Subsonic Civil Airplanes*. John Wiley & Sons, 2013.
- [42] MR Van Der Toorn. "Flying-V Family design for stability and control". In: *Delft University of Technology* (2022). URL: <http://resolver.tudelft.nl/uuid:c9c1ded2-a0a0-4e95-9d81-5d93e9f54ad2>.